University of Tennessee, Knoxville
TRACE: Tennessee Research and Creative Exchange

Doctoral Dissertations | Graduate School

8-2014

# Monte Carlo Modeling of Ion Beam Induced Secondary Electrons

Uk Huh
*University of Tennessee - Knoxville*, uhuh@utk.edu

Follow this and additional works at: https://trace.tennessee.edu/utk_graddiss

 Part of the Other Materials Science and Engineering Commons

## Recommended Citation

Huh, Uk, "Monte Carlo Modeling of Ion Beam Induced Secondary Electrons. " PhD diss., University of Tennessee, 2014.
https://trace.tennessee.edu/utk_graddiss/2832

This Dissertation is brought to you for free and open access by the Graduate School at TRACE: Tennessee Research and Creative Exchange. It has been accepted for inclusion in Doctoral Dissertations by an authorized administrator of TRACE: Tennessee Research and Creative Exchange. For more information, please contact trace@utk.edu.

To the Graduate Council:

I am submitting herewith a dissertation written by Uk Huh entitled "Monte Carlo Modeling of Ion Beam Induced Secondary Electrons." I have examined the final electronic copy of this dissertation for form and content and recommend that it be accepted in partial fulfillment of the requirements for the degree of Doctor of Philosophy, with a major in Materials Science and Engineering.

David C. Joy, Major Professor

We have read this dissertation and recommend its acceptance:

Claudia Rawn, David Keffer, Haixuan Xu

Accepted for the Council:

Carolyn R. Hodges

Vice Provost and Dean of the Graduate School

(Original signatures are on file with official student records.)

# Monte Carlo Modeling of Ion Beam Induced Secondary Electrons

A Dissertation Presented for the
Doctor of Philosophy
Degree
The University of Tennessee, Knoxville

Uk Huh
August 2014

**Dedication**

This dissertation is dedicated to my parents, Mannhee Huh and Hyekyung Moon.

## Acknowledgements

Completion of my study with a Ph.D. degree is possible entirely with the help of my research advisor, Dr. David C. Joy. I truly appreciate his time, guidance, recommendations, insight and encouragement for helping me to grow to be a better scientist.

I express my sincere gratitude for financial support from the Center for Materials Processing in UT during my Ph.D. study. My research was partially supported by the center.

I am particularly grateful to Dr. Claudia Rawn, Dr. David Keffer, and Dr. Haixuan Xu for accepting the responsibility to serve on my committee.

## Abstract

Modeling ion beam induced secondary electron (iSE) production within matter for simulating ion beam induced images has been studied. When the complex nature of ion beam interactions with matter is account for, a detailed quantitative model of the ion interactions with matter, Monte Carlo simulation will be the best choice to be able to compute and predict iSE yields faster and more accurately. In order to build Monte Carlo simulation software incorporated with a reliable database of stopping power tables, for wide variety of range of materials, there have been numerous attempts to experimentally measure ion stopping power tables and to tabulate the data. Experimental data for pure elements and compounds is almost totally absent and the ability of advanced software to calculate iSE production within matter for producing reliable predictions is limited. Despite the need having a complete set of experimental ion stopping power tables will not be easily obtained for at least several decades. This study explores the incorporation of a universal stopping power curve, calculated and published by the National Institute of Standards and Technology at Boulder, into a Monte Carlo simulation software that will be able to compute iSE yield for both pure elements and compounds. This new approach of modeling iSE generations for pure elements and compounds will contribute to quantify performance of the helium ion microscope and other ion microscopes.

## Table of Contents

## List of Tables

## List of Figures

# Chapter 1

# Introduction

## 1.1. Why do this study?

This study is necessary to quantify the performance of recently commercialized helium ion microscopes by creating and building a quantitative model of ion interactions. Ion beam induced secondary electron yield (iSE δ) is one of the most important parameters for enabling imaging of helium and different types of ion microscopes. iSE δ influences the imaging quality of microscopes in many aspects including depth of field, spatial resolution, and contrast. iSE carries chemical, topographical, and contrast information of the near surface of matter studied. Hereafter, high iSE δ efficiency will make it easy for detector to collect and read the signals carrying various information from materials so that helium ion microscope will be able to make it possible for everything in region of interest or frame to be in focus, for any closely located scanned lines to be resolved in an image, and for grey scale to be resolved in many finer steps.

To predict and interpret generation of secondary electrons by ions for matters in reliable precision, Monte Carlo simulation has been known for one of the best statistical method to simulate scattering events of energetic ion behavior in matter due to fast and accurate calculation for the complex ion beam interactions with matter [1].

To enhance the Monte Carlo simulation, more accurate information of ion stopping power tables for wide range of materials is necessary because the database of the tables should be able to determine below aspects that will affect iSE generation behavior; geometric spatial distribution of interaction volume and ion beam induced secondary electrons emitted in and out of matters, iSE yield efficiency, and etc. for

material of choice. However, not enough theoretical data and almost total absent data of ion stopping power for pure elements and, even further, compounds has been reported. We may not have any high quality measured secondary electron yield data for any materials at any energy with very little error bar even after more than ten years.

**1.2. My Contribution**

So far, several research groups have pursued individual data tables for helium ion stopping power by calculating and measuring with several different kinds of statistical models and experimental techniques [2-5]. However, having every set of data through experiments is extremely difficult when limited number of world wide research facilities where these extremely expensive and technologically demanding experiments can be performed are considered. Even further, access to these research facilities is also not-readily-open to every truth seeking researchers and scientists no matter how user proposals are written in convinced matter and turned in. Even worse, research funds that can run these expensive experiments are very limited and not enough at all in these economic sequester prevailing all over the world. When difficulties of the experiments to collect data tables of 'pure elements' for helium stopping power are claimed to be almost so miserable already, attempts to have data tables of 'compounds' will be impossible when countless number of existence of compounds materials are considered.

All or almost enough individual data tables for helium stopping power may be fully acquired someday, however no body will be able to assure when time comes. The time may be too late when there exists highly emerging demand for the data tables of helium stopping power of both pure elements and compounds and these data tables need to be ready pretty soon.

So, instead of relying on hundreds of individual experimental data tables of helium stopping power, a recently calculated and published result by the group at NIST at Boulder will be exploited. The group at NIST at Boulder recently published database of helium ion stopping power as a function of energy for both several elements and compounds in Figure 1.1.

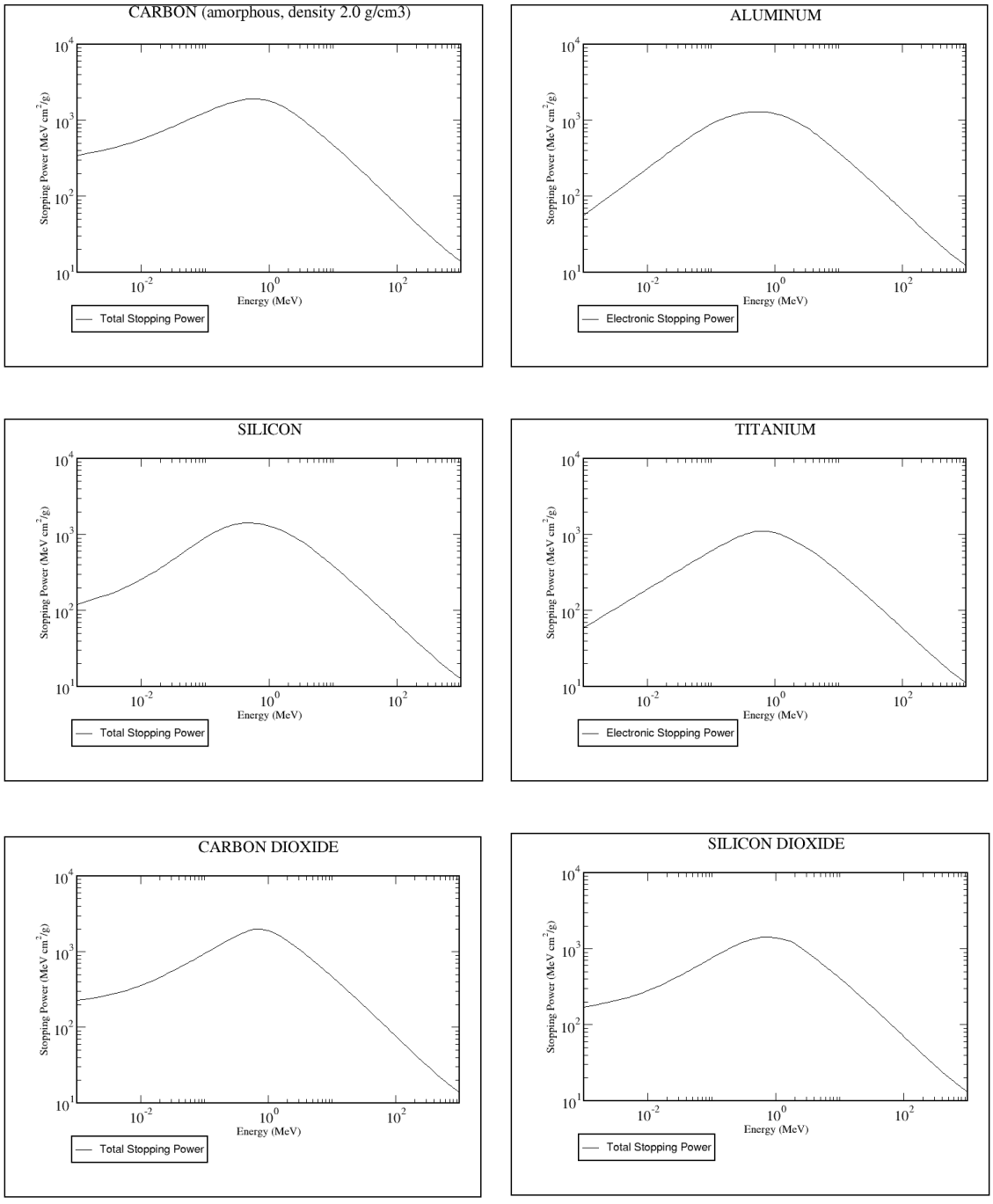


Figure 1.1. Stopping power of C, $CO_2$, Si, $SiO_2$, Al, and Ti for helium ions [6]

At even very short glance at the database, it is immediately obvious the shape of the helium ion stopping power curves is almost same and its intensity stays within

reasonable range of order for several materials including even complex materials as well as pure elements. With this close resemblance of each stopping power curves, new idea to invent a universal curve for helium ion stopping power as a function of energy referring to database presented by the group at NIST as Boulder came up. It will be a big contribution to the study of modeling ion beam induced secondary electrons if universal curve for the helium ion stopping power should be able to be incorporated into Monte Carlo simulation software so that the software will be able to compute and predict iSE yields for both pure elements and compounds in wide range of beam energies.

Overlays of the stopping power curves for He ions clearly indicates there is very little difference in stopping power between pure elements and compounds in terms of the shape of the stopping power curve, and its absolute intensity in Figure 1.2. This result is important because it shows that the velocity of the incident ions, and the density of the target material are far more important than the chemistry of the sample in determining the yield of iSE.

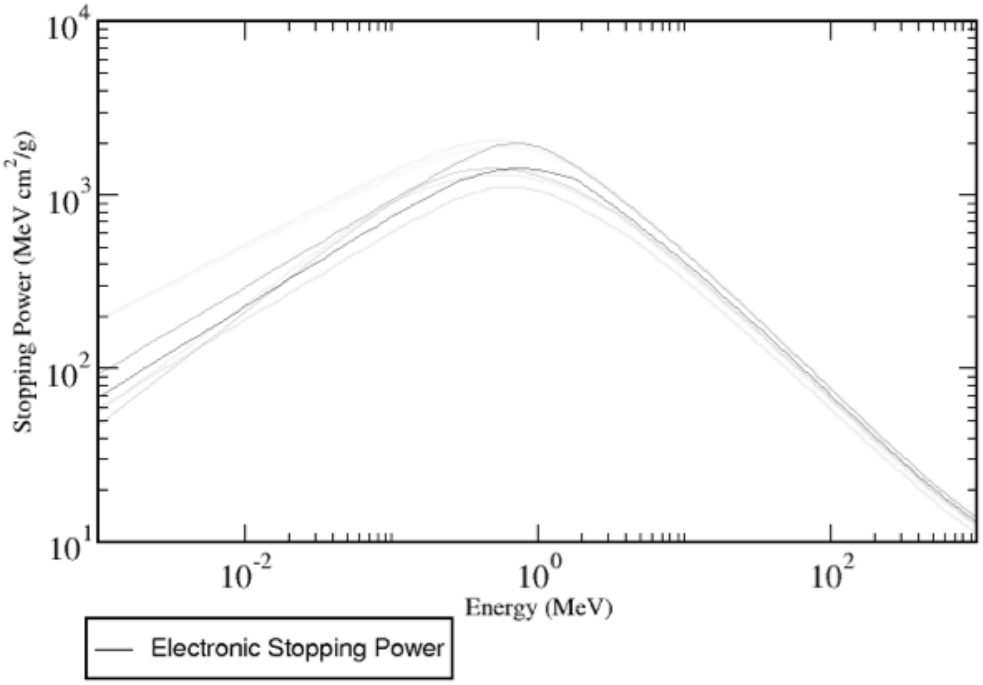


Figure 1.2. Overlays of stopping power curves for He ions

Not like SEM that typically uses < 1keV of incident electron beam, $He^+$ beam energy of helium ion microscope is approximately 40 keV because interactions of swift particles with solids depends on their velocity not their energy. A helium ion is 7,297 times heavier than an electron so that 5 eV of electron has equivalent velocity to 40 keV of helium ion, which enables similar degree of interactions of electrons and ions with solids.

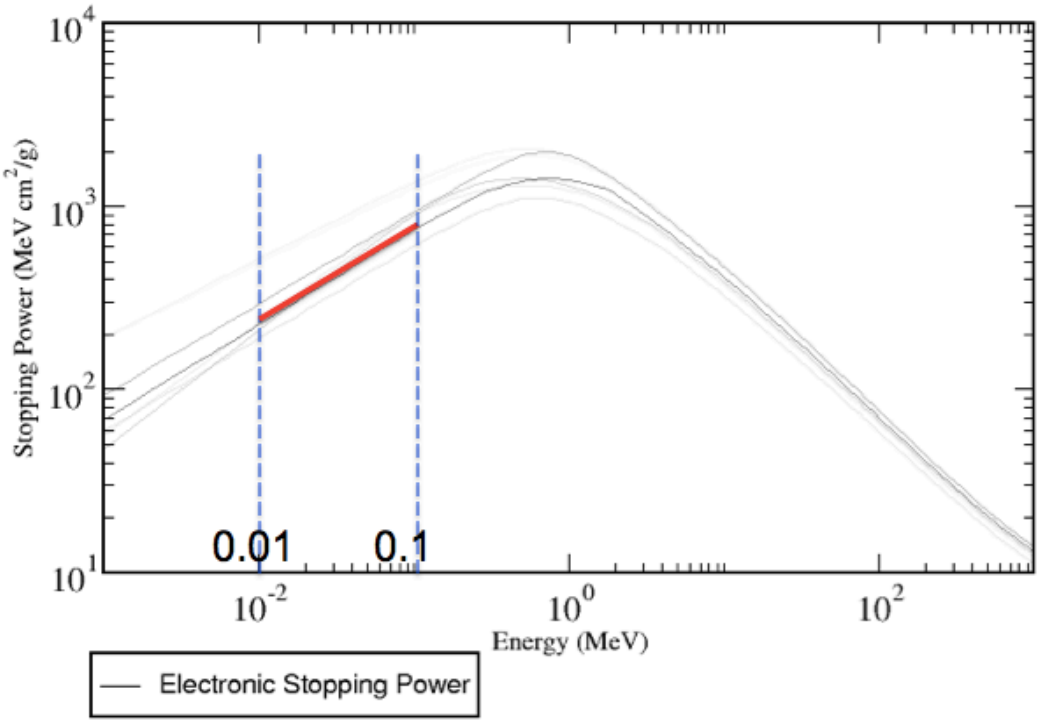


Figure 1.3. 1st approximation of curve at range of interest

To have a universal curve at range of interest, effective energy range of practical helium ion beam in use between 10 and 100 keV is picked up. This range will be able to cover all the versatile explore of the helium ion beam machine for several different applications. 1st approximation of the curve occurs within the range (10~ 100 keV) and it is indicated as red solid line in Figure 1.3.

To a good approximation (10% of better) it has been shown that there is the universal curve for helium ion stopping power as a function of energy within ion beam range between 10 and 100 keV in Figure 1.4. This data curve will be called 'Universal ASTAR Curve' for helium ion stopping power and used in the Monte Carlo simulation to compute the iSE δ. The universal ASTAR curve for helium ion stopping power as a function of incident ion energy x (0.01 MeV ≤ x ≤ 0.1 MeV) is approximated by the equation 1.1.

$$\mathbf{(dE/dx)}_{\mathbf{electronic}} = -1E{+}09x^6 + 4E{+}08x^5 - 7E{+}07x^4 + 6E{+}06x^3 - 321859x^2 + 18491x + 54.323$$

(Equation 1.1)

And, even further, it is very important that the universal curve should be able to be applied to both pure elements and compounds because the theoretical and experimental stopping power tables of the helium ion stopping power published by the group at NIST at Boulder shows there is very little difference in stopping power between pure elements and compounds in terms of the shape of the stopping power curve, and its absolute intensity. This result is important because it shows that the velocity of the incident ions, and the density of the target material are far more important than the chemistry of the sample in determining the yield of iSE.

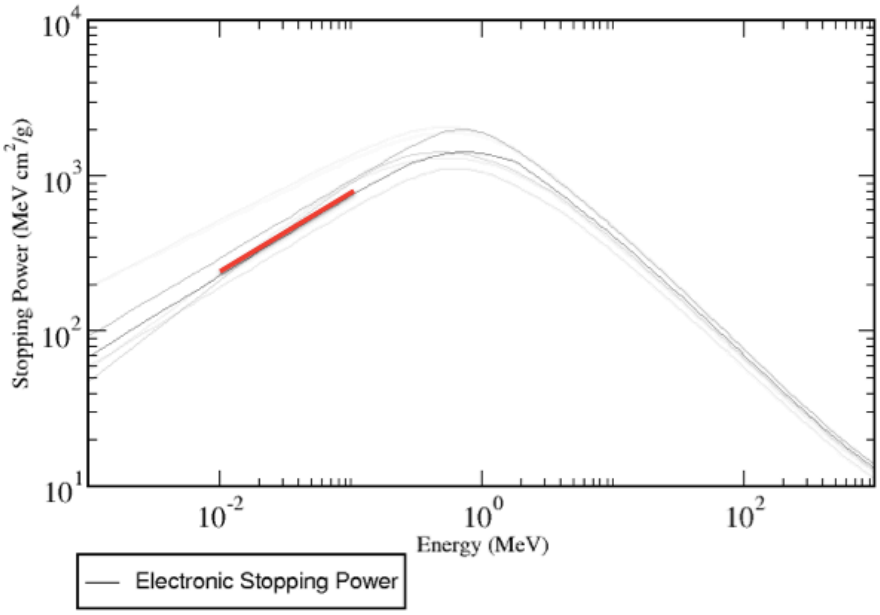


Figure 1.4. Universal ASTAR curve of stopping power for He ion

Adoption of the universal curve to the Monte Carlo simulation software may not be a perfect solution for computing helium ion beam induced secondary electron behavior within matters, but given the almost absence of high quality experimental data of helium ion stopping power, understanding the iSE behavior within range of error bars (10 ~ 15 %) is a big step forward and contribution to the current helium ion beam metrology. The advanced Monte Carlo simulation will enable to predict the range of the incident helium ion beam, predict the fraction of the signal that is backscattered (SE1/SE2), and predict lateral and vertical distribution of ions that come to rest within the target so that the simulation software will model helium ion induced SE production within matters (both pure elements and compounds).

The universal yield curve for helium ion induced SE emission will enable us to understand the iSE behavior in not only pure elements but also compounds better. Furthermore, our new approach should be able to handle not only helium ion beam but

also other ion beams by simply changing the basic scattering profile. Hereby, it is believed that our new approach will be a milestone to enhance capabilities and performance of the currently commercialized helium ion microscope, and even further, other ion microscopes.

### 1.3. Hypothesis & Proposition

The use of universal ASTAR curve of helium stopping power as a function of energy in the Monte Carlo simulation initiates with a proposition that the helium stopping power tables recently published by NIST Boulder [6] are both the most complete and accurate theoretical data set of stopping power currently available and the use of the universal ASTAR curve implies this idea is very important because it shows that the velocity of the incident ions, and the density of the target material are far more important than the chemistry of the sample in determining the iSE δ. Figure 1.1 shows stopping power data for helium ions in a variety of materials, and it is immediately obvious that there is very little difference in stopping power between pure elements and compounds in terms of the "shape" of the stopping power curve, and its absolute intensity. This result also provides an immediate solution to calculating the iSE yields from compound materials, which so far has not been possible. The overlay of all the available curve of stopping powers, $1^{st}$ approximation of curve at the range of interest, will be able to be applied to both pure elements and compounds to model iSE production within matter. This approach is not being proposed as a perfect solution to the problem of simulating ion beam induced images but, given the almost total absence of high quality experimental data, this approach is currently the best estimate as shown in Equation 1 and Figure 1.4. Our enhanced Monte Carlo simulation software incorporated with the universal ASTAR

curve will make it possible to predict iSE yields for both pure elements and compounds in wide range of energies.

For accurate and fast calculation of ion beam induced secondary electrons, Monte Carlo modeling with the continuous-slowing down approximation approach will be adopted in recording the Monte Carlo simulation software. Dapor shows both Monte Carlo simulations adopting the energy straggling strategy and the continuous-slowing down approximation give identical simulation results from interaction between ion beam and matter in agreement with experimental data in Figure 1.5 & 1.6, however Monte Carlo modeling based on the continuous-slowing down approximation incorporating stopping power of materials shown in equation 1.2 was order of magnitude faster [1].

$$\delta = -1/\varepsilon_s \int \frac{dE}{ds}\, e^{\frac{z}{\lambda s}}\, dz \qquad \text{(Equation 1.2)}$$

(δ: secondary electron yield,
$\varepsilon_s$: secondary electron excitation energy,
dE: energy loss,
dS: segment of trajectory,
z: depth
$\lambda_s$: effective escape depth)

The continuous-slowing-down approximation approach only spends 25 seconds of time of computation while the energy straggling strategy requires more than 300 seconds because the former approach uses reduced number of physical parameters while the latter takes account of entire physical phenomena. The former uses only two whilst the

energy straggling strategy does the four. The ion beam induced secondary electron yields should be able to be calculated more accurately and quickly than the Monte Carlo codes with entire details of physical phenomena involved in the secondary electron generation (inelastic collisions between ion and target atoms and cascade of secondary electrons); energy, lateral, depth, angular distribution of the emitted electrons, angular dependence and primary energy dependence of the secondary electron yield [1].

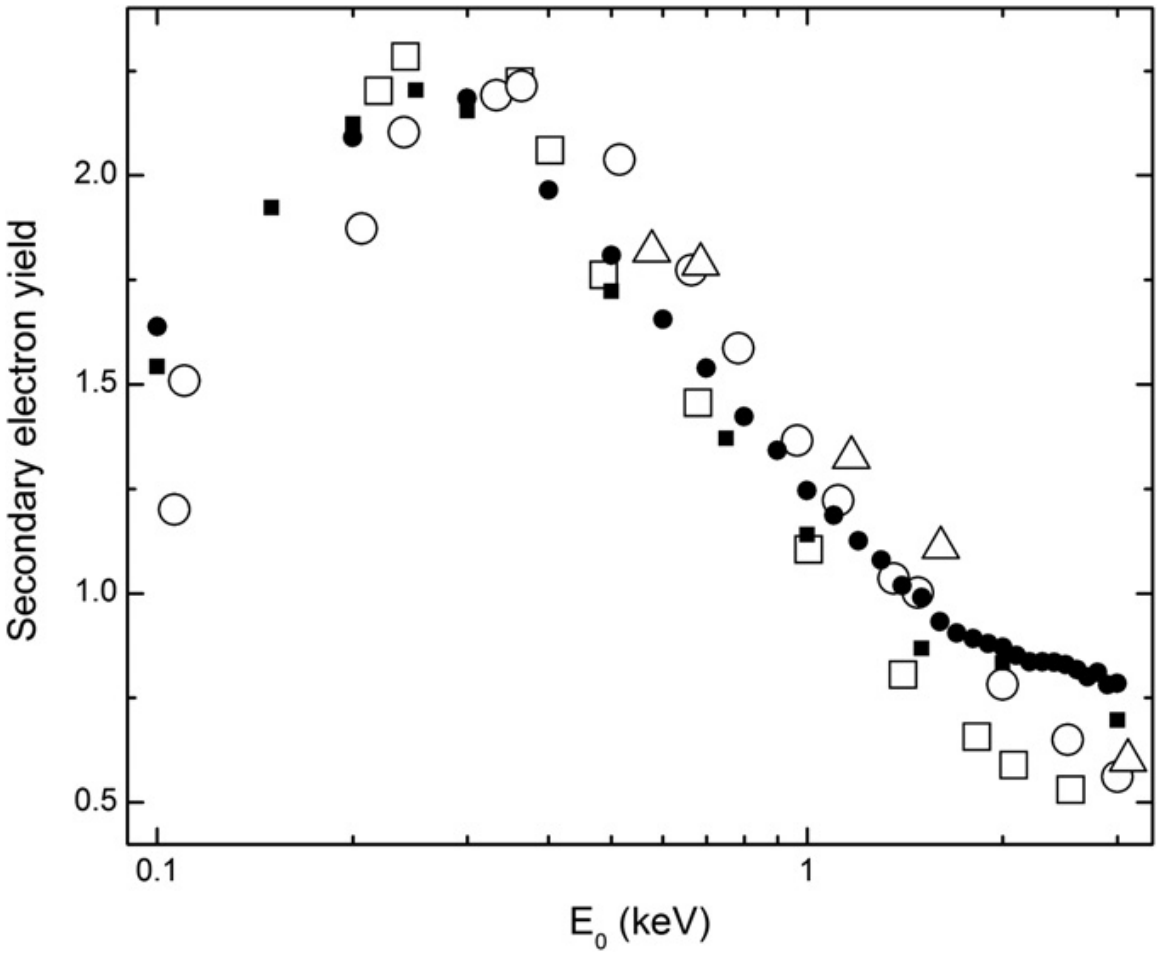


Figure 1.5. Comparison between Monte Carlo calculations and experimental data of polymethylmethacrylate secondary electron yields as a function of the primary electron energy. Filled squares represent the present Monte Carlo calculations based on the energy straggling strategy. Filled circles represent the present Monte Carlo calculations based on the continuous-slowing-down approximation. Empty squares are the Matskevich experimental data. Empty circles are the Boubaya and Blaise experimental data. Empty triangles are the Rau et al. experimental data [1]

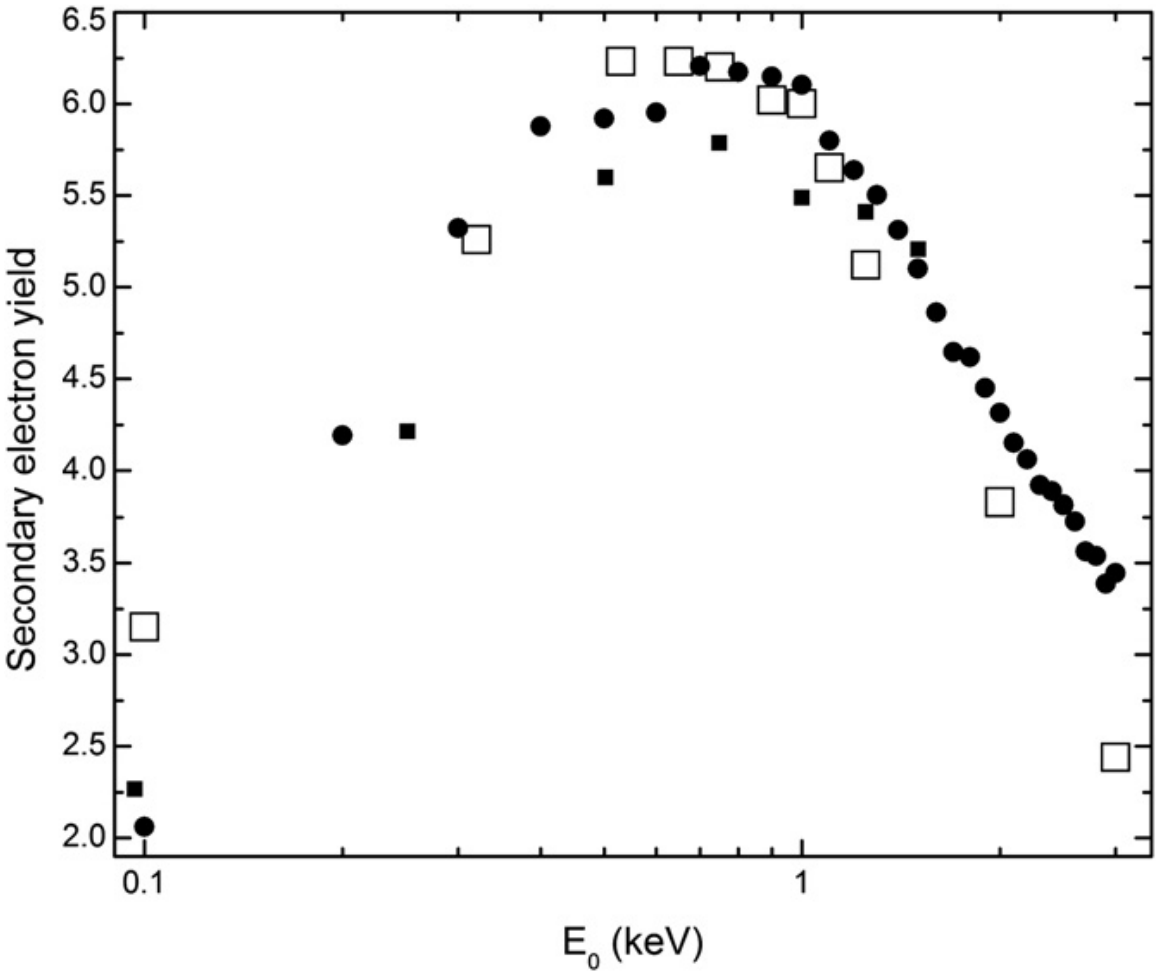


Figure 1.6. Comparison between Monte Carlo calculations and experimental data of $Al_2O_3$ secondary electron yields as a function of the primary electron energy. Filled squares represent the Ganachaud and Mokrani Monte Carlo calculations based on the energy straggling strategy (Wph = 0.1 eV, C = 1.0 nm_1, c = 0.25 eV_1, v = 0.5 eV). Filled circles represent the present Monte Carlo calculations based on the continuous-slowing-down approximation (es = 6.0 eV, ks = 1.5 nm). Empty squares are the Dawson experimental data [1]

# Chapter 2

# Literature Review

## 2.1. Advantage of HIM over SEM

Helium ion microscope (HIM) is a next generation microscope making it possible to image, characterize, and nanofabricate nano-sized materials never been practicable with the traditional scanning electron microscope for higher resolution imaging and many other applications. The HIM uses a beam of helium ions as the imaging particles, not electron beam, as stable helium ion imaging source is successfully developed by ALIS Corporation. Newly invented ion source makes possible to emit single atom from a sharp needle's apex maintained under high vacuum in cryogenic temperature when electric field is applied. The protrusion of single atom in the Atomic Level Ion Source (ALIS) emitter enables high brightness ($4 \times 10^9$ A/cm$^2$/sr) since the single protruded atom carries all the ion currents. This helium ion beam has approximately 1% shorter DeBroglie wavelength than electron beam since the electron is 7,800 times heavier than the helium ion in mass, so that electron's smaller momentum gives rise to 86 times longer wavelength than helium ion of the same energy. This short DeBroglie wavelength makes it possible to form almost parallel converged beam with little influence by diffraction effects, so that this result in high depth of field. The smaller wavelength of the helium ion also makes probe size smaller and its probe size reaches down to 0.50 nm. For each incoming helium ion from 2 to 8 secondary electrons are generated while one secondary electron is produced for each incoming electron at the SEM. This abundance of secondary electrons makes the HIM to have high contrast imaging available. Even more, interaction volume induced by helium ion-solid interaction is much smaller and narrower than that for the SEM. SE imaging from localized region of interest in specimen allows higher spatial resolution and accurate material analysis. For

TEM analysis, sample preparation procedure is tedious and requires special facilities and experience. Even with these environments for sample preparation ready, the procedure is somewhat tricky and it is also possible to lose sample during the preparation by chance. The HIM does not require these complicated sample preparation procedure and even better, imaging is possible with no further surface coating on specimen, which may be non-conductive materials though[7, 8].


Figure 2.1. Commercialized helium ion microscope by Carl Zeiss

Figure 2.2 illustrates cross-sectional view of the end-form of a field ion tip of conventional field ion microscope (FIM) and helium ion microscope (HIM). Those two microscopes adopted same fundamental idea to use gas field ion sources to emit ion from the apex of sharp needle held at high positive voltage in the presence of a gas.

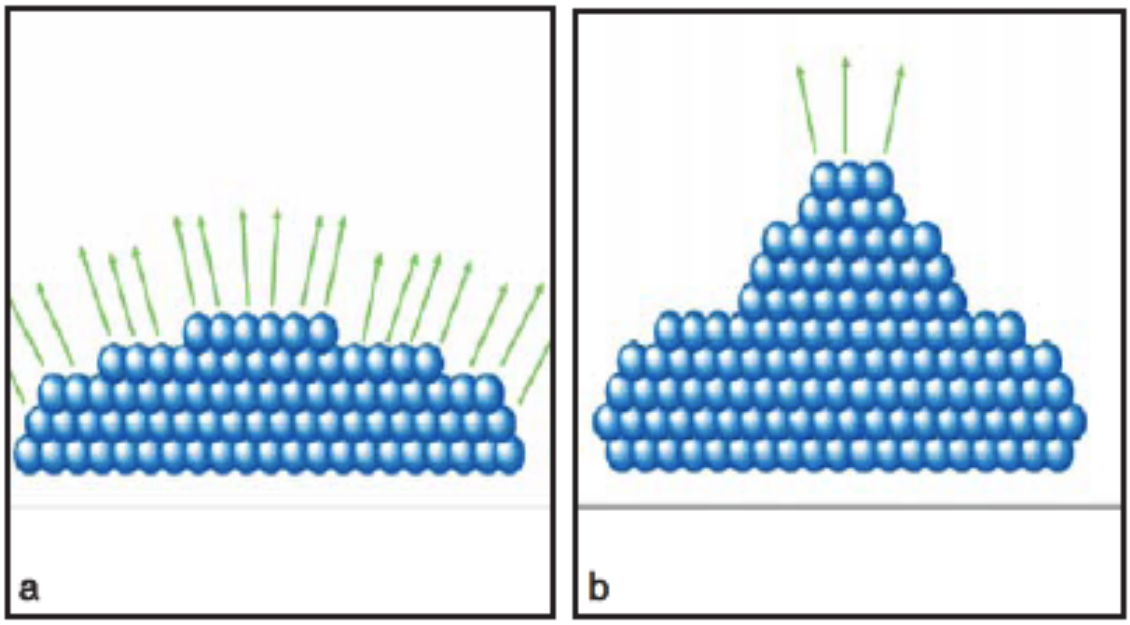


Figure 2.2. Comparison and contrast between end –form of field ion tip and ALIS emitter (a) Illustrated cross-sectional view of the end-form of a field ion tip (b) Illustration of the ALIS emitter [7]

While hemispherical end form of ion emitter needle allows ions formed on the top of each atomic shelves of the emitter to be emitted, HIM was built on invention of new type gas field ion source, maintained under high vacuum in cryogenic temperatures, which makes it possible to form a few single atoms at the very top of sharper distal end of the ion emitter [9]. In connection with geometry of the Atomic Level Ion Source (ALIS) emitter tip having conical shape, a few single atoms (TRIMER) are formed on the very top of the atomic shelf of the emitter and single atom is protruded when appropriate voltage is applied, which enables to have smaller beam spot size (0.5 nm) and higher brightness (> 4 X $10^9$ A/$cm^2$ sr) than conventional gas field ion sources. Actual geometries of the FIM tip and the ALIS emitter are imaged in Figure 2.3 and it is

immediately obvious that distal end of ALIS emitter forms a few atoms, which should be able to contribute to smaller beam spot size.

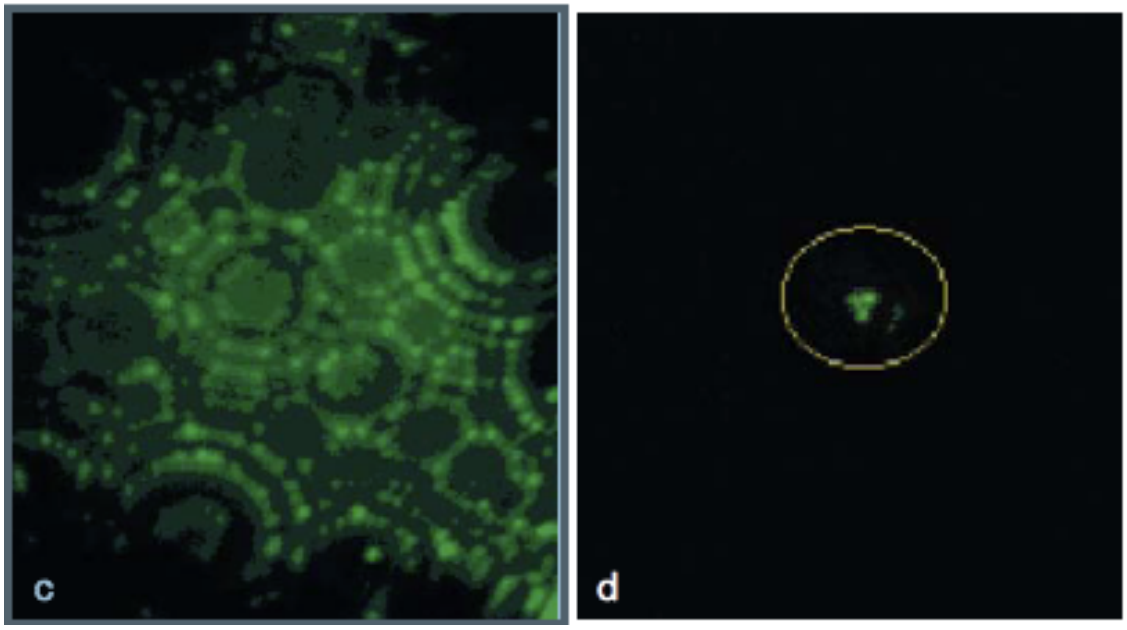


Figure 2.3. Comparison and contrast between actual tip of field ion microscope (FIM) (c) Actual tip image of the geometry illustrated in Fig. a (d) Actual tip image of ALIS emitter illustrated in Fig. b [7]

In addition to small spot size given by invention of single atom emission through the ALIS emitter tip, de Broglie wavelength, λ, of helium ion beam used in the helium ion microscope is almost 1% less than that of electron beam of the same energy (Figure 2.4), so that collimated ion beam should be able to form almost parallel converged

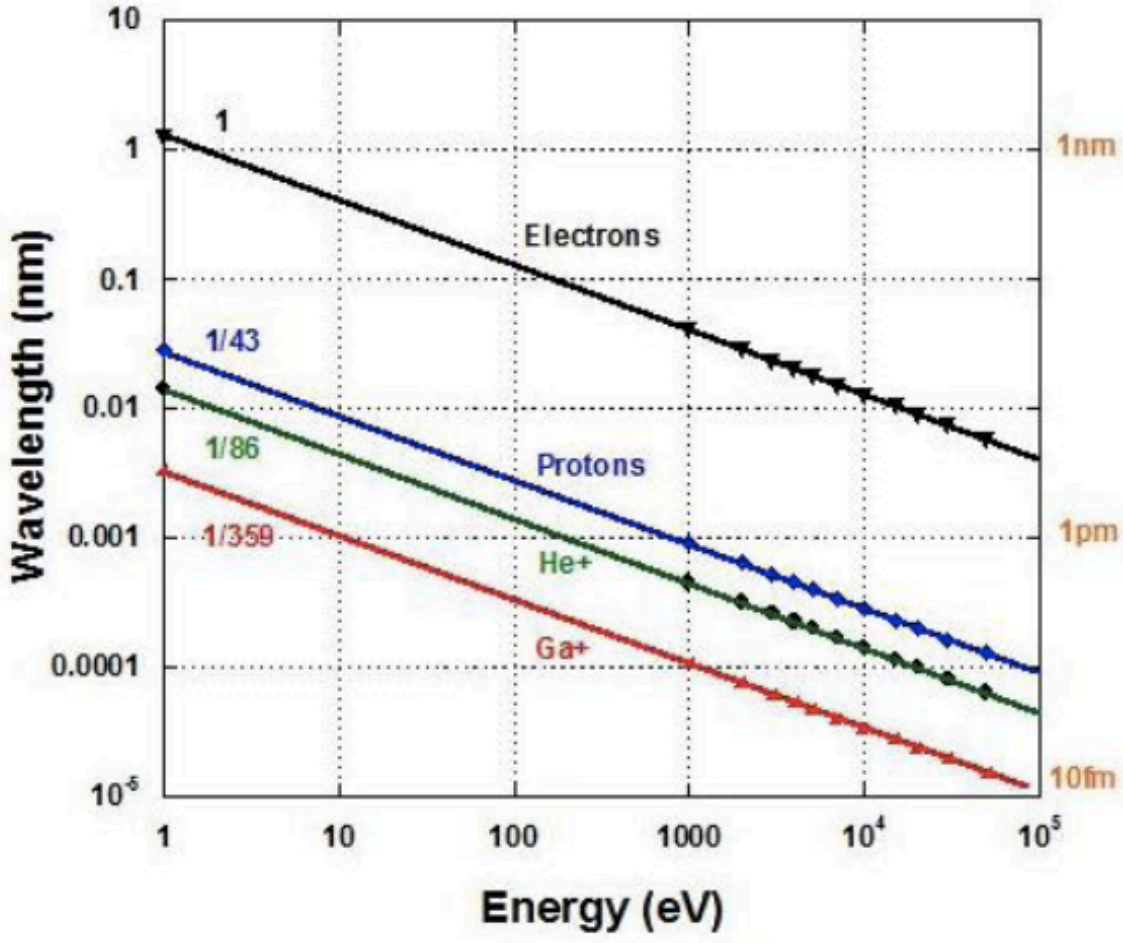


Figure 2.4. Wavelength (nm) of electrons, and protons, helium and gallium ions, as a function of energy

beam with much less influenced by diffraction effects than case of electron beam. This short wavelength of helium ion beam makes it possible to produce small convergence angle, α, of the beam (less than 0.1 mrad), so that scanning probe is formed in a shape of a finely sharpened needle in conjunction with geometry of ALIS emitter tip. This small spot size of the helium ion microscope from geometry of ALIS emitter tip and small

wavelength of helium ion beam results in superb depth of field with a finely sharpened probe, and with no compromise, high spatial resolution as well [8, 10].

This small size and ultra-sharp shape (small convergence angle) of probe of helium ion beam should be able to scan nearly every region of interest, which may have quite non-consistent longitudinal heights or three dimensional complex structures or nano-sized pores, cracks, and crevices where there has been difficulty to place a probe formed by electron beam in those sites. As secondary electrons are produced by interaction of the probe with the surface of specimen, these secondary electrons carrying the information of specific places will be collected by detector to form SE imaging and these abundant acquisition of the secondary electrons contribute to high depth of field. The imaging performance for extremely complicate specimen so far wasn't so impressive with relatively larger size of probe from the electron beam. Blurred features present backward in the image are observed as scanning probe would not be capable of reaching deep enough, which is determined as 'not-in-focus'. Figure 2.5 indicates everything in the image is in focus even for complex three-dimensional structures with use of HIM. Presence of nano-sized pores in organic matters, highly plausible material formed from thermally altered residual petroleum, having spongy appearance was identified with clear determination of size of the pores. This has not been plausible with use of conventional SEM so far. Surface detail and depth of field into the image are significantly noticeable and good virtue of using HIM (Figure 2.6).

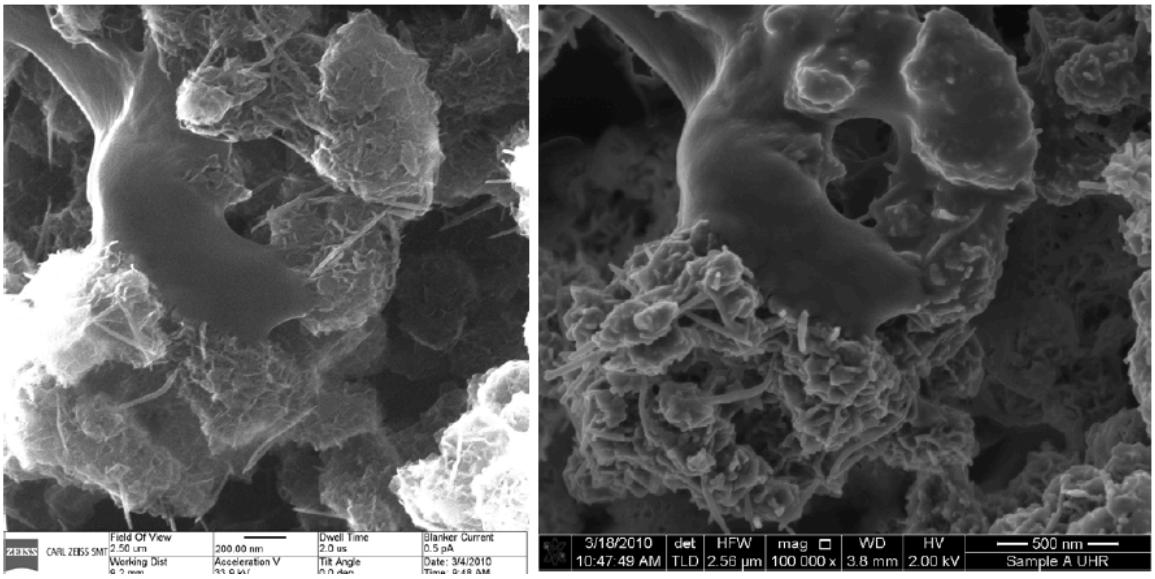


Figure 2.5. HIM (left image) provides imaging of fragile 3D structures with higher spatial resolution, depth of field, and material contrast than SEM (right image) [11]

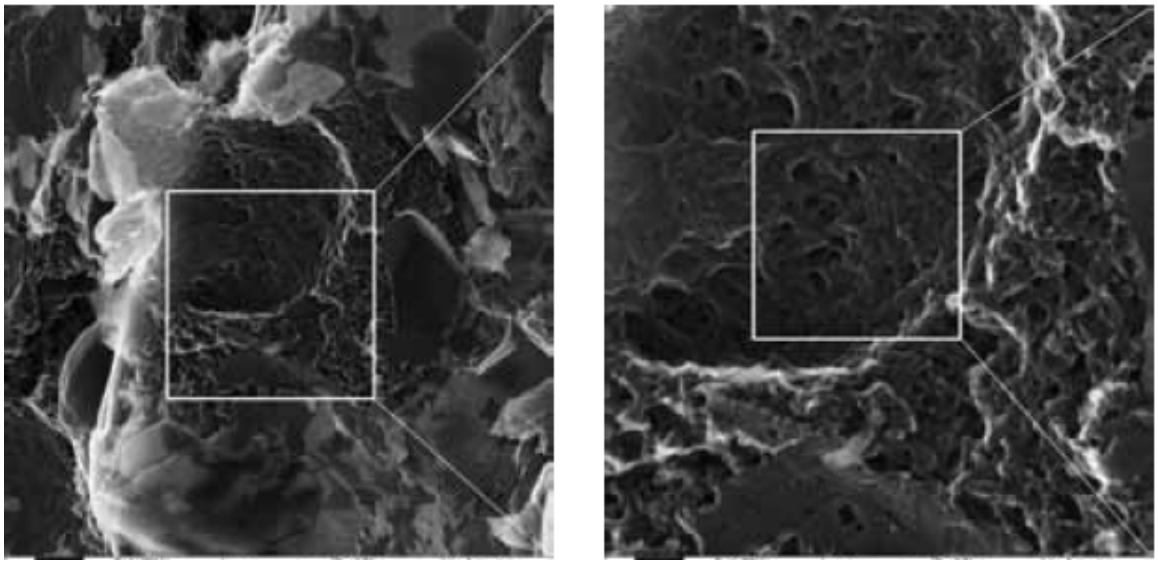

Figure 2.6. Images of Middle Otter Park Shale from Horn River Basin. Pores are as small as 2nm [12]

Effective generation of iSE[#] signals is another virtue of HIM. Higher secondary electron yield makes it easy for detectors to collect ion beam induced secondary electrons and

form SE images as a result, better signal to ratio is maintained contributing to high resolution. This higher yield is produced an order of magnitude than SEM since energy loss for ion beam is stronger than that for electron beam. This higher secondary electron yield, i.e. wider range of secondary electrons, gives rise to expression of wider range of gray level in images. In conjunction with capability of producing wider range of gray level, iSE yield is a function of material than SEM, so that excellent material contrast could be observed with quite distinctive expression of gray levels between different materials. Good material contrast between two different materials is presented as a result of comparing the same image using two different microscopes (Figure 2.7 & 2.8). Different materials are used inside the aligned cross than the outside. When aligned cross is imaged by the SEM, not a quite distinctive material separation is observed. Two different materials could be differentiated in an image based on abundant SE signals when the HIM is utilized; excellent material contrast is shown with distinctively different gray levels between the inside and outside aligned cross.

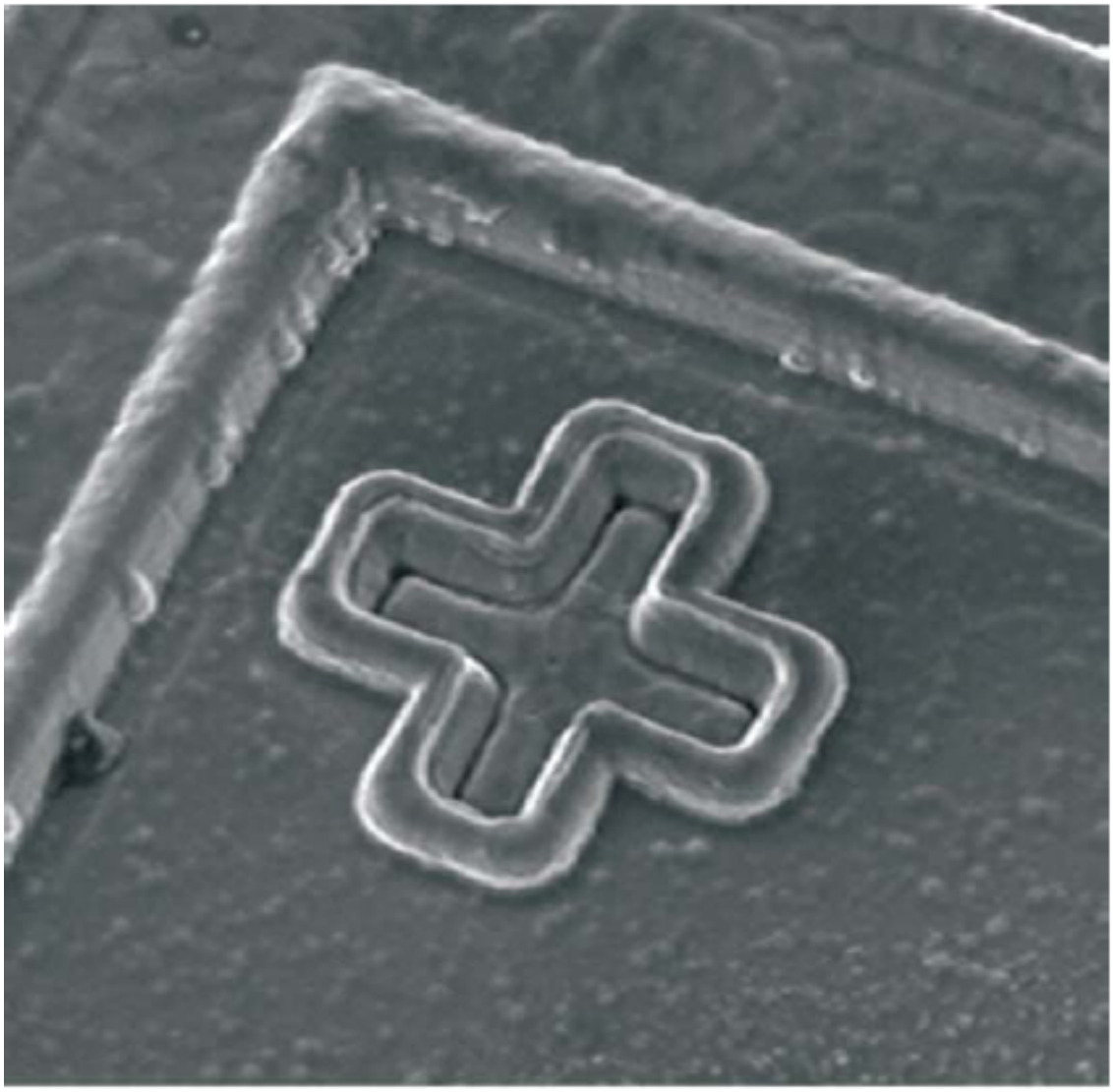

Figure 2.7. Secondary electron SEM image of aligned cross [8]

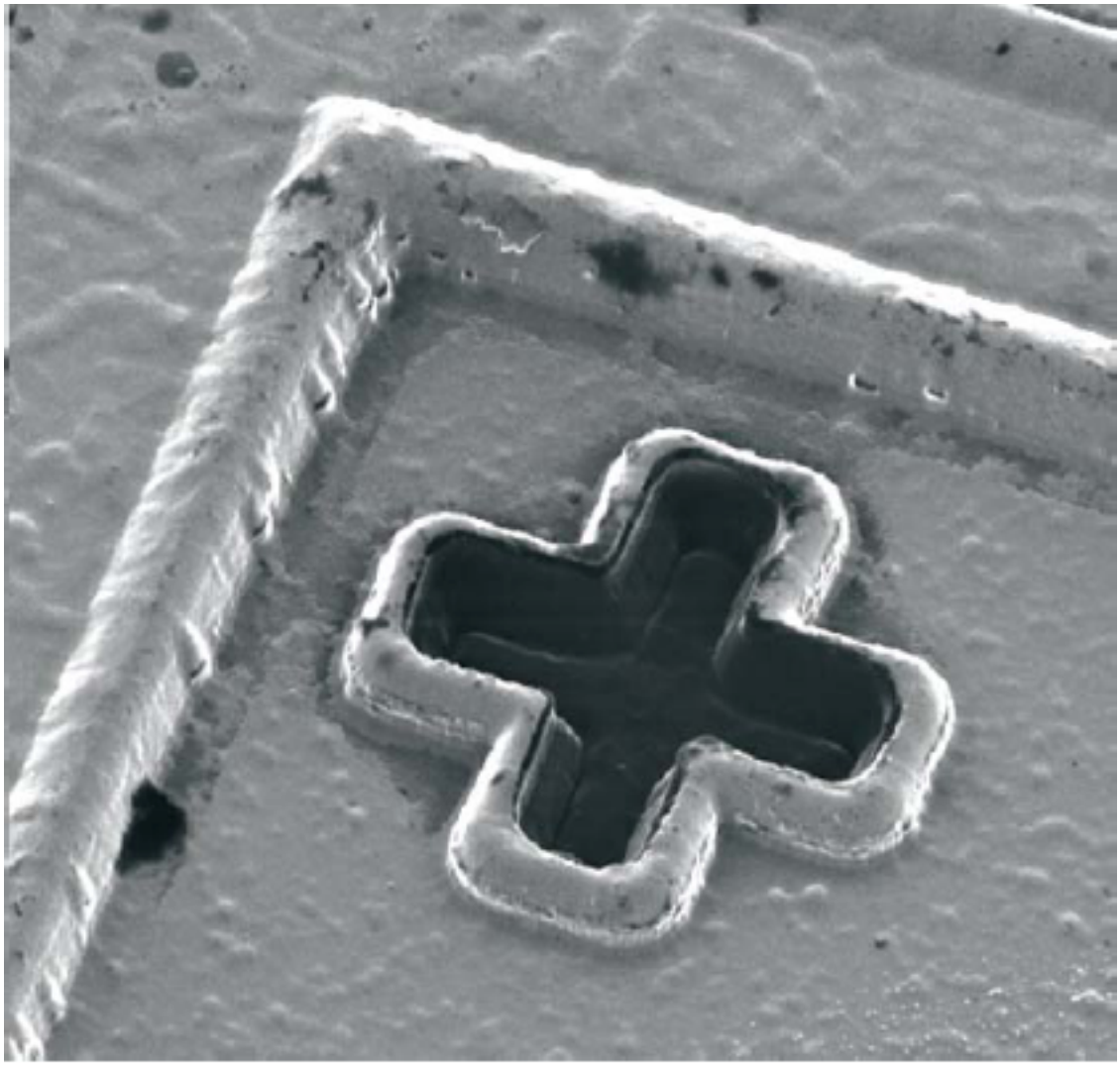

Figure 2.8. Secondary electron ALIS image of same alignment cross [8]

Another good example of material contrast given by the HIM is a chemically patterned, self-assembled monolayer of nitrobiphnyl thiol (NBPT) formed on a gold film (Figure 2.9). HIM makes it possible for the patterned monolayer to be differentiated from the gold film, and even further, not olny this material separation but also visualization of the NBPT monolayer has never been successful with use of the SEM.

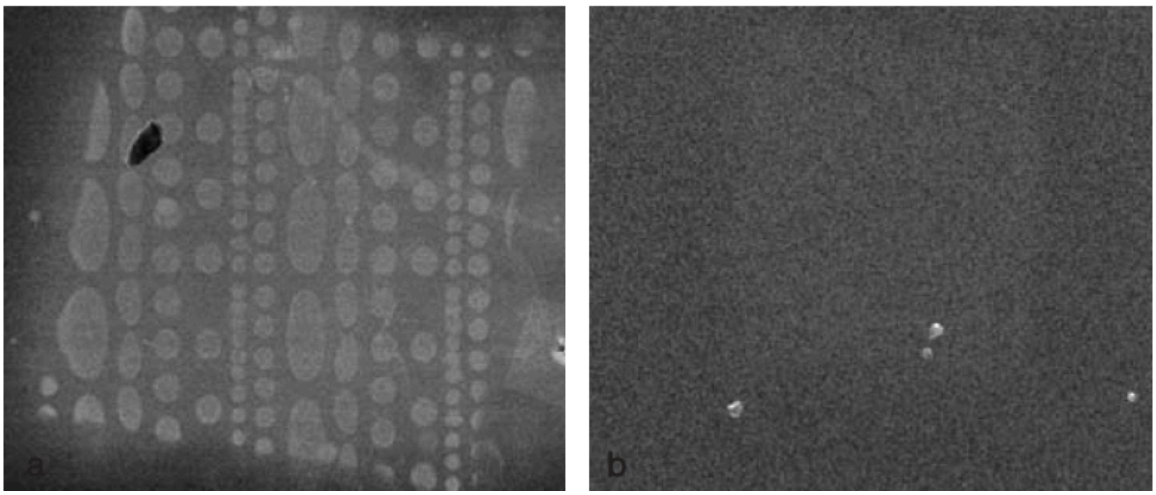


Figure 2.9. NBPT monolayer over a gold film, patterned with an electron beam mask (Left) HIM image, (Right) SEM image [7]

In addition to the material contrast realized with high secondary electron yield, Rutherford backscattered ion images (RBI) provides atomic number contrast, sensitive to atomic number difference, by collecting backscattered ions through detector, which uses different channel than SE detector. The Z contrast signal is complementary to SE signal, so that it should be able to provide better material and chemical contrast.

While forming images of samples with electron beam necessarily requires deposition of conductive layer on the specimen, imaging non-conductive materials with no additional treatment of specimen, for example, coating or low vacuum environment, is possible using helium ion microscope. Right image in Figure 2.10 shows Mo whiskers grown on substrate could be imaged where no special surface treatment was provided.

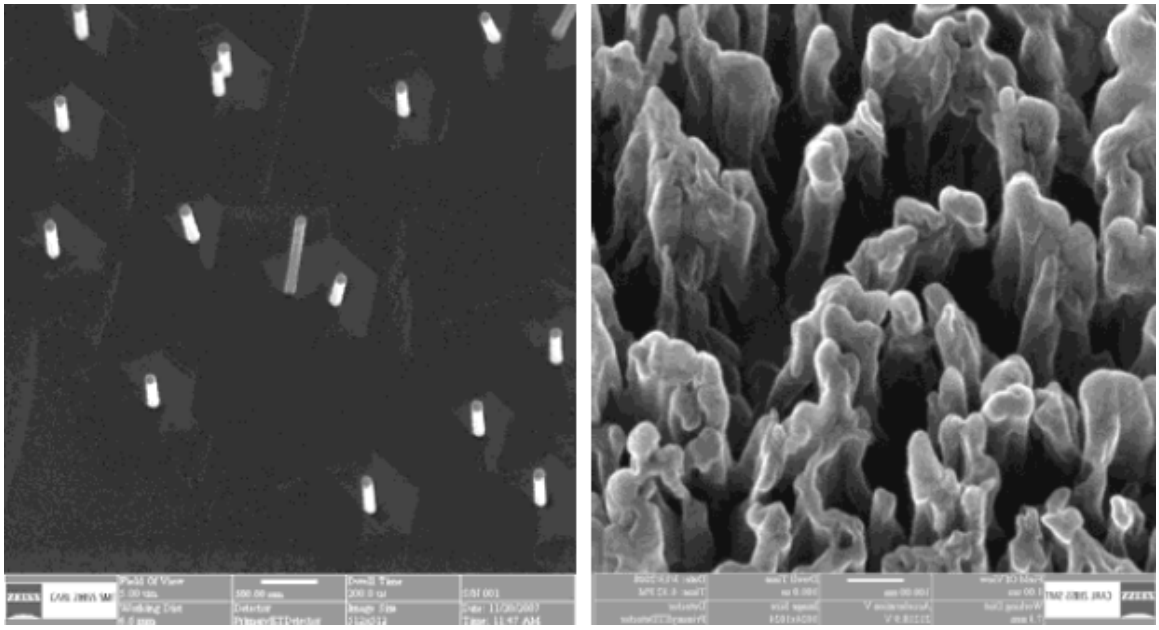

Figure 2.10. (Left) Images of InAs nanowires showing SE contrast, (Right) Mo whiskers on substrate [13]

## 2.2. Secondary Electrons

### 2.2.1. Definition of Secondary Electrons

Secondary electrons are defined as emitted electrons produced by energetic electron, proton, or ion irradiation to matters and energy of those emitted electrons is less than 50 eV. Secondary electrons are defined purely on the basis of their kinetic energy; all electrons emitted from the specimen with energy less than 50 eV are considered as secondary electrons. Complete energy distribution of electrons emitted from specimen is schematically illustrated in Figure 2.11. The energy ranges are divided into two regions; firstly, where most of secondary electrons are distributed from 0 to 50 eV, and where backscattered electrons are distributed from 50 to energy of incident electrons beam [14].

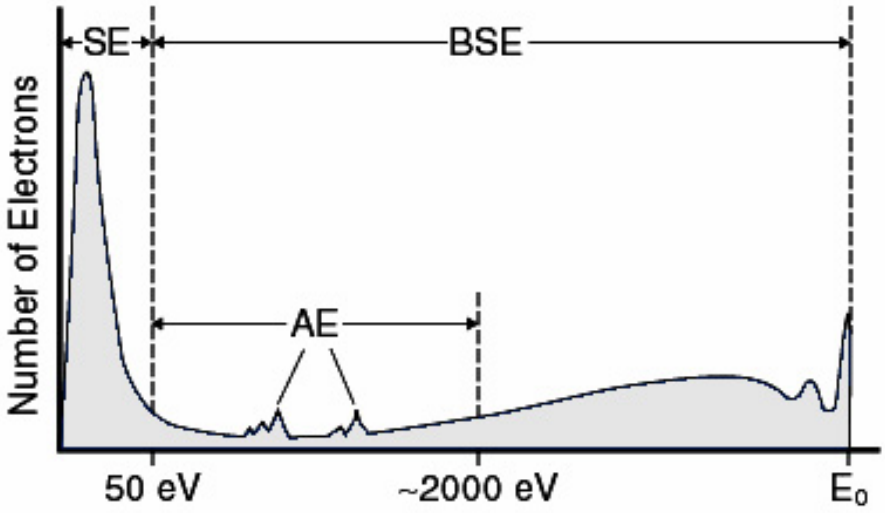


Figure 2.11. Energy distribution of secondary electrons [15]

Figure 2.12 illustrates these secondary electrons are located originally at the outer shell of target atoms and are able to be detached from the shell when enough kinematic energy to loose the bound from the incident beam is given to the shell during inelastic scattering of energetic beams. In metal, electrons bound weakly at conduction band are going to be emitted as a result of ion-atom interaction, inelastic scattering, and called secondary electron. Secondary electrons in semiconductors and insulators will be produced at electrons at outer shell valence electrons [14].

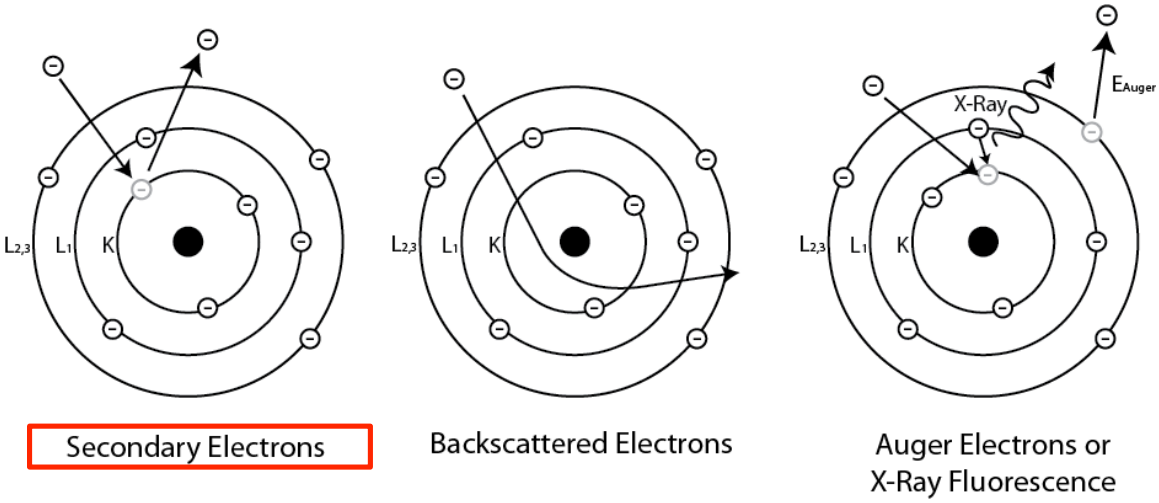


Figure 2.12. Schematic diagrams of emission of electrons in the k-orbital of matter's atom

### 2.2.2. Escape of Secondary Electrons

Secondary electrons may travel within the matters and, as a consequence, escape through the surface of matters. The secondary electrons are produced along the ion beam trajectories within specimen, however the produced secondary electrons, with

their low kinetic energy, will not escape the matter if they lose all the energies during their propagation within the specimen due to their intrinsic nature of inelastic scattering, which shows gradual energy loss through passage. Surface potential barrier should be overcome for secondary electrons to reach and escape the surface, so that they should possess at least several electron volts, which is required kinetic energy to overcome the work function of specimen and escape the specimen [14]. In addition, the maximum effective escape depth of secondary electrons was determined 5λ (λ, mean free path of secondary electrons) [16].

### 2.2.3. Type of Secondary Electrons

When incident ion bombards the specimen and starts interaction with target atoms, secondary electrons are produced within ε (=5λ) in Figure 2.13 and they escape through the specimen surface. The $SE_1$ originates at and near to the ion-solid interaction location and the signal could come from deep in the sample. These secondary electrons are called $SE_1$. The $SE_1$ signal carries high-resolution signal, which should be able to provide highly surface sensitive information. After incident ion travels within the specimen, it may reach the surface and pass through it. For this instance, secondary electrons produced within ε (=5λ) in Figure 2.13 would escape through the surface of specimen. These are designated as $SE_2$. This signal could originate micrometers from the initial ion-solid interaction location. The $SE_2$ signal, in contrast, carries low-resolution signal than $SE_1$ does. While operating scanning electron microscope, the backscattered electrons may hit the pole piece and, as a result, secondary electrons could be produced from the hit location. These secondary electrons are designated as $SE_3$. The information present in the $SE_3$ signal is quite different than $SE_1$ and $SE_2$. This complex nature secondary electron makes it difficult to build Monte Carlo modeling [13, 14].

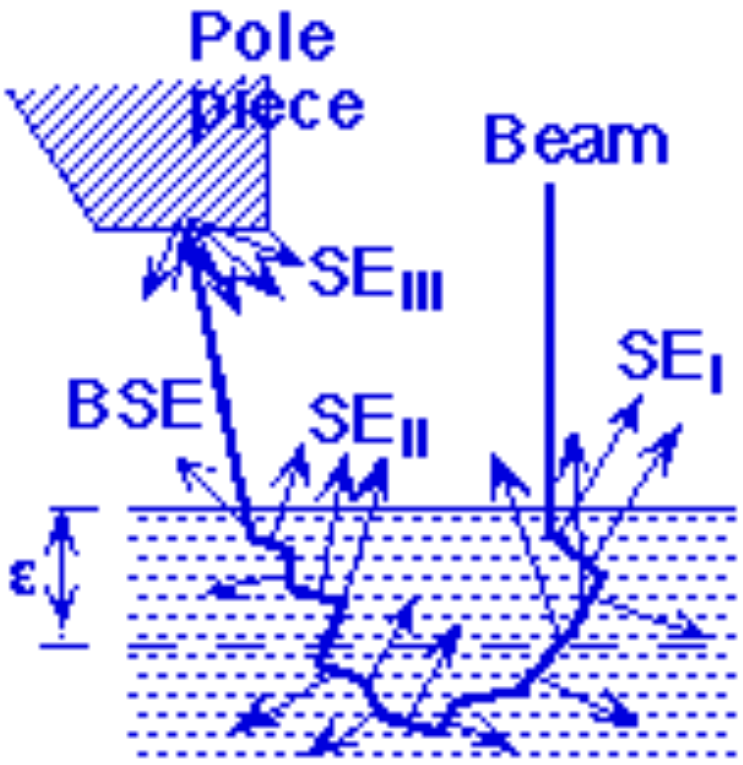


Figure 2.13. Schematic diagram of generation of $SE_1$ and $SE_2$ [17]

### 2.2.4. Importance of Secondary Electrons

The emitted secondary electrons are the most conventionally used imaging mode in scanning electron microscope and helium ion microscope for the past decades. The emitted secondary electrons carry chemical, topographical, and contrast information of near surface of matters so that detailed information of materials can be given. Due to the small size of interaction volume measuring characteristic of materials in specific and isolated range is possible; high spatial resolution is one of good virtue. As shown in Figure 2.14, high yield efficiency enables the detector easy to collect and read the signals carrying various information from materials [14].

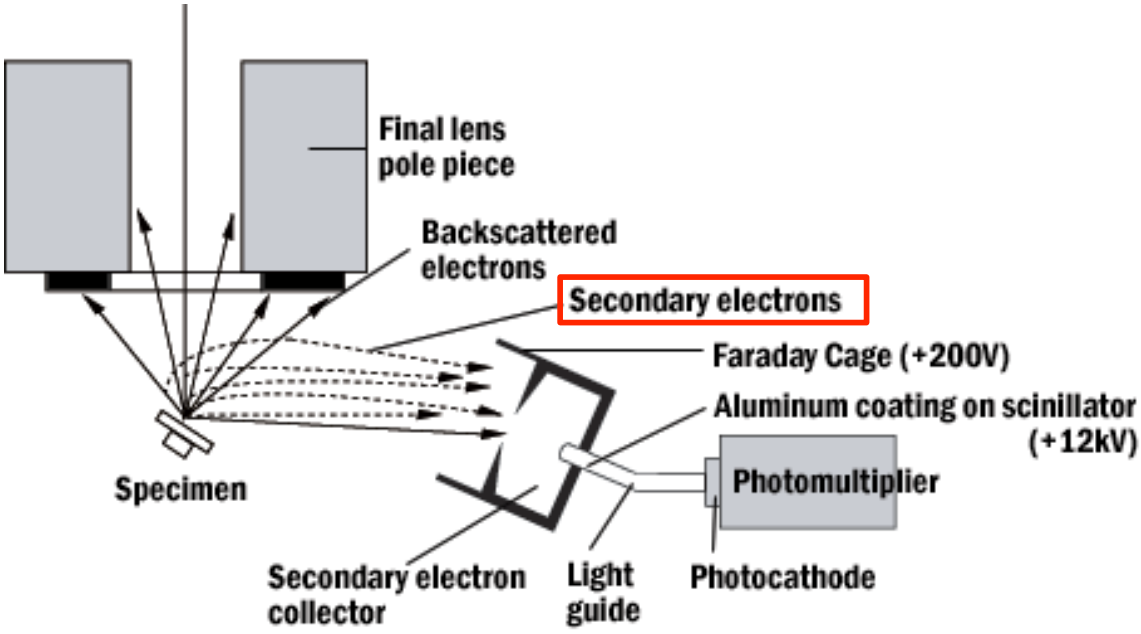


Figure 2.14. Diagram showing the recording of information about a specimen in a scanning electron microscope [18]

**2.3. Interaction Volume**

When energetic ion enters matter it experiences interactions with target atoms of matter. The incident ion may experience collisions with the nucleus of the specimen atoms and cause elastic scattering; the positively charged incident ions collide the positively charged nucleus of target atoms so that this should be able to make the incident ions to travel in deflected manner, to all possible direction with no kinetic energy loss (Figure 2.15). The probability of this elastic scattering event, scattering cross

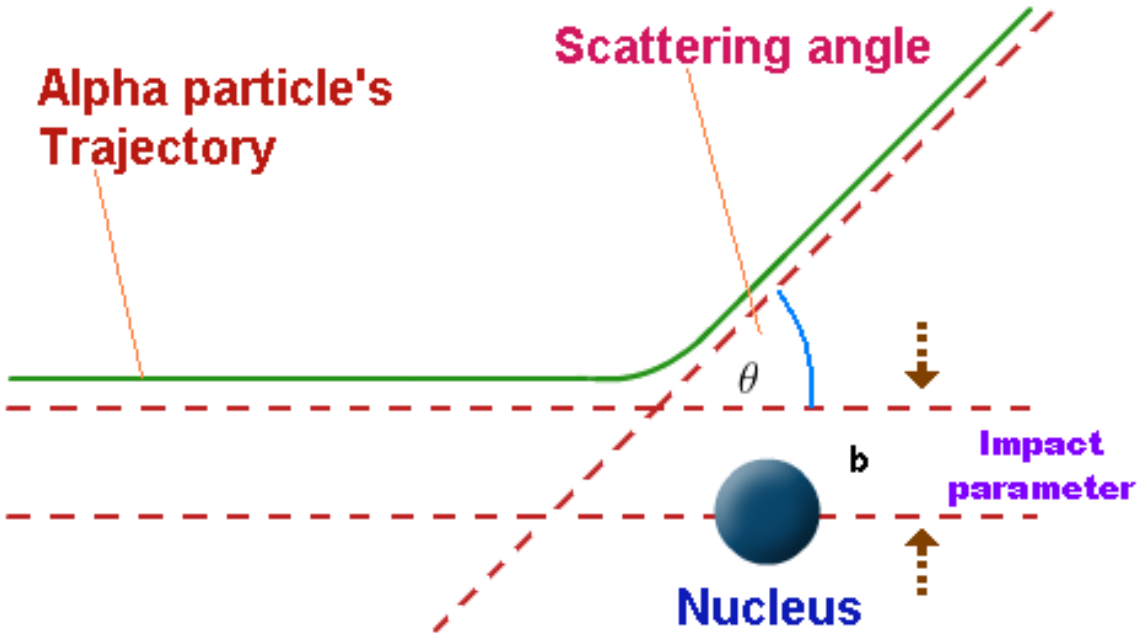


Figure 2.15. Elastic scattering process when alpha particle strike to positively charged nucleus due to electrostatic force of repulsion [19]

section, $\delta_c(\theta_c)$ will be increased as atomic number of target atoms increases or energy of incident ion decreases. Elements with higher atomic number will have higher Rutherford scattering cross section while decrease in ion energy will result in higher Rutherford scattering cross section as shown in Equation 2.1.

$$\delta_c(\theta_c) = Z_1^2 Z_2^2 e^4 / 16E^2 \sin^4(\theta_c/2) \qquad \text{(Equation 2.1)}$$

At the same time the incident ion experiences elastic scattering events, it also lose and gain its charges during it travels through the electron clouds of atomic shells of target atoms; the incident ion loses its energy and transfer the energy to target atoms gradually during its propagation through atom layers until the incident ion loses all of its energy and finally, takes place to rest. This scattering event is classified as inelastic scattering (Figure 2.16).

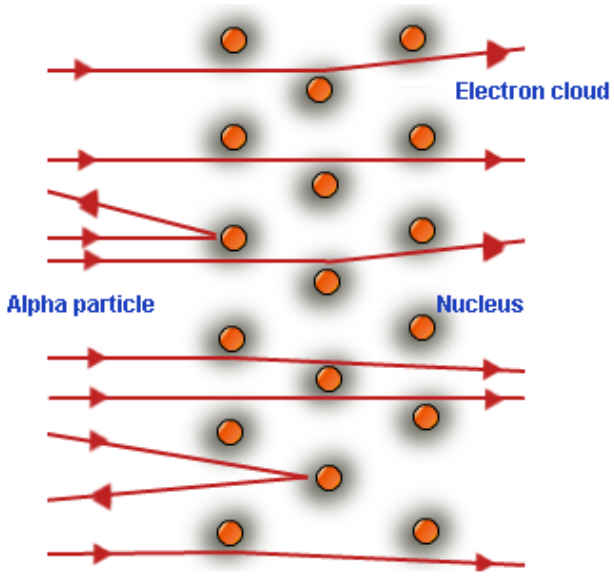


Figure 2.16. Inelastic scattering process when alpha particle enters negatively charged electron cloud [19]

With the previously described elastic and inelastic scattering events given by the ion interactions with matter, the specimen experiences ion beam induced damage as shown in Figure 2.17, presenting electron-specimen interaction, it is obvious that fundamental

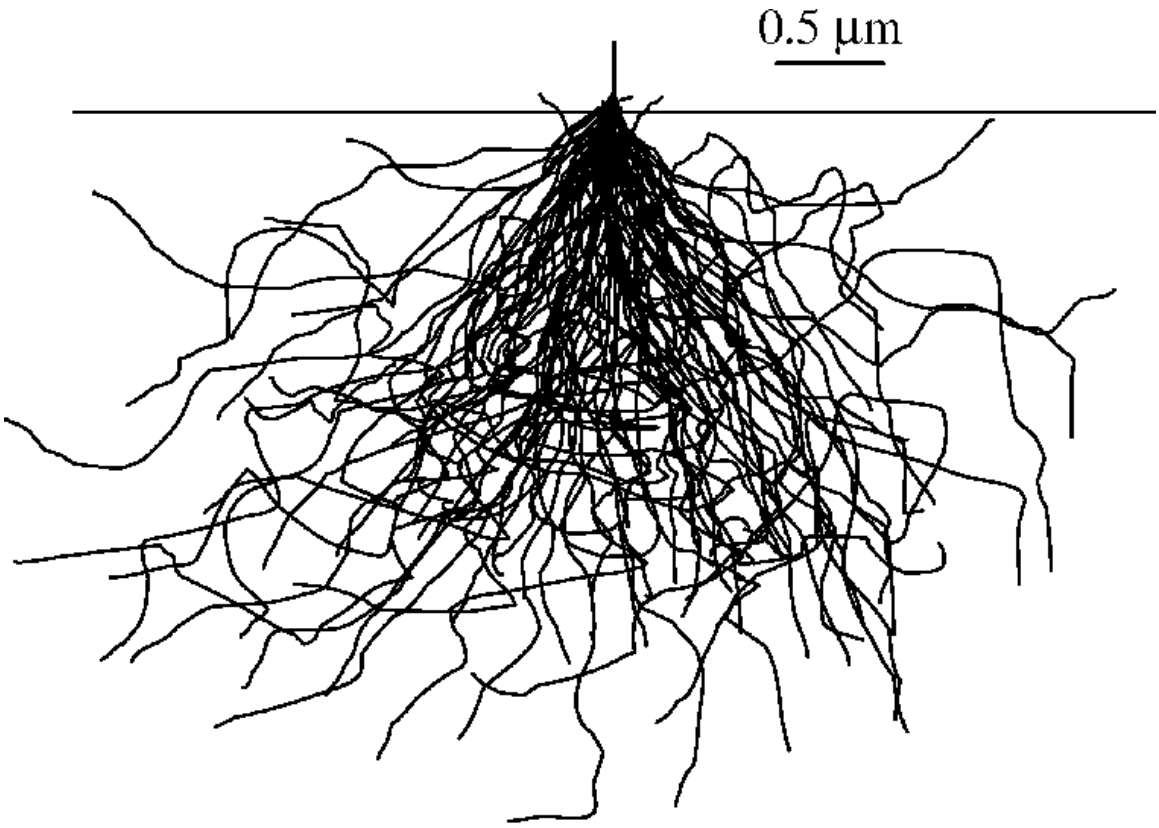


**Source:** Joy (1995)

Figure 2.17. Interaction volume and depth penetration (from Monte-Carlo simulation) for a sample-based carbon [20]

concept of scattering events is quite similar to the case of ion-specimen interaction. At each trajectory of incident ions, the particle interacts with specimen all the time until it comes to rest within matter; this interaction, in turns, should be able to be expressed as

ion beam induced damages on the matter. This damaged region is called ‘interaction volume’ where makes it possible to produce secondary electrons, which is essential signals used for forming images in electron and ion microscopy. The range, size, shape and lateral distribution of the damaged region are highly dependent on incident particle energy and kind of target material. The ion beam damage is proportional to the deposited energy to the material. As incident beam energy is increased, the size of the damaged region, interaction volume is enlarged when same material and density of the material is used. This gives rise to higher chance to produces secondary electrons. Influence of atomic number and specimen surface tile on the interaction volume was also reported, however the influence of beam energy on the interaction volume is far more significant.

Secondary electron from the interaction volume is such an essential signal used for forming images in electron microscopy and high degree of understanding the ion-matter interaction process in the interaction volume is necessary in interpreting SEM images. To compute the effect of elastic and inelastic scattering events during the ion-matter interactions, occurring in the interaction volume, Monte Carlo simulation technique has been introduced because some of important physical parameters in the scattering model vary over a range of values in a totally unexpected manner; for instance, the scattered ion after any kind of collision with an atom will proceed in a certain step length until the ion encounters another atom. After another collision, the ion will move forward in another step length in unpredicted directions until the ion encounters next atom. These ion trajectories will be stretched to zigzag shape like Brownian movement until the ion lose all of its energy in Figure 2.18. The scattering angle in each step length of the trajectories of will be total random from 0 to 180 degrees.

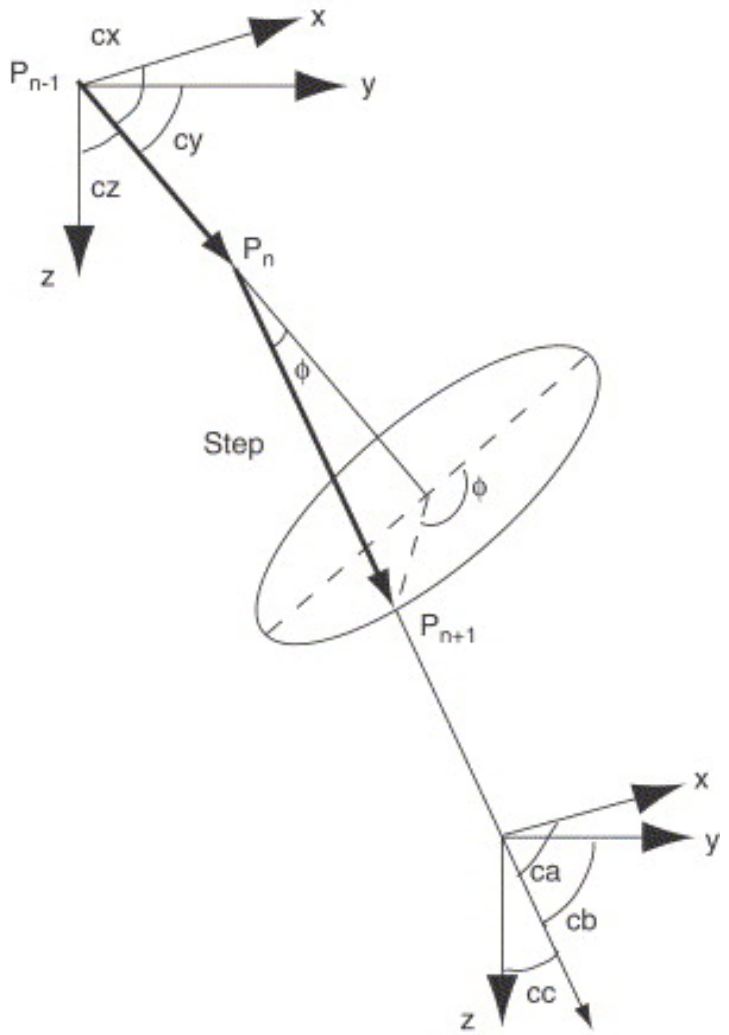


Figure 2.18. Definition of coordinate system used in the Monte Carlo simulation program [20]

This characteristic of random scattering angle brought the necessity to adopt the idea of using random numbers that should be able to produce the appropriate statistical distribution of the physical events. This use of random numbers brought an immediate attention to adopt Monte Carlo simulation technique to compute the scattering events given by ion-atom interactions. Modeling the trajectories of ion followed by the

scattering events will be a fundamental foundation for computing the lateral distribution of deposited energies (interaction volume), which will be able to contribute to calculate the ion beam induced secondary electron yield. Monte Carlo simulation technique is believed to compute the secondary electron yield, which will lead to interpret the SEM images formed by secondary electron imaging. Not like many of ion beam induced rays secondary electrons only produced at the near surface will be collected by the detector to form image. As the effective escape depth of secondary electron is of nanometer scale, secondary electrons produced at the depths deeper than a few nanometers will be lost in the matter and will not be emitted out of the specimen. Even further, interaction volume of the helium ion microscope in Figure 2.19 is much smaller than that of scanning electron microscope with the same velocity of energetic particle. Henceforth, ion beam induced secondary electrons should be able to carry chemical, topographical, and contrast information of small surface area (horizontally), and near surface (vertically) of matter. So, obtaining the secondary electrons carrying various information from material will give rise to in-depth examination of materials in aspect of chemical composition analysis, structural analysis, microanalysis, and so on with much better spatial resolution, depth of field, and material contrast.

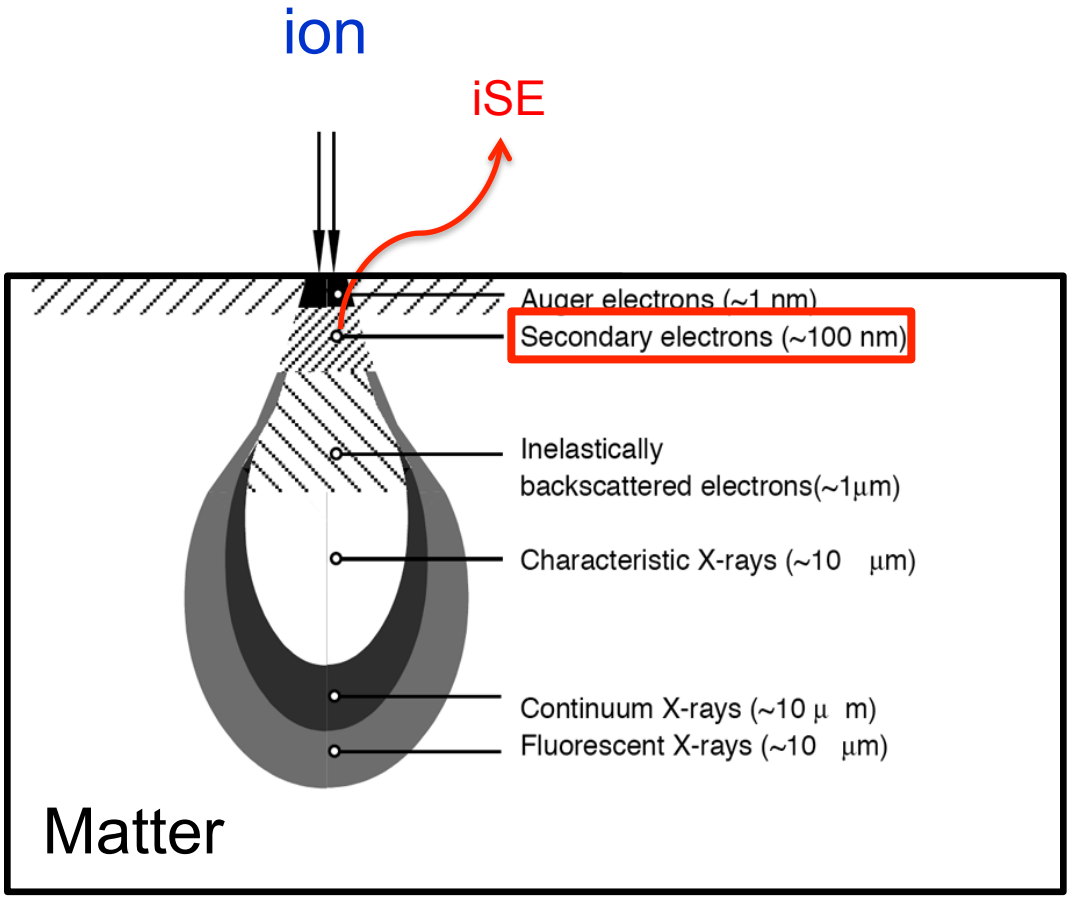


Figure 2.19. Specimen interaction volume during helium ion microscope analysis [21]

## 2.4. Stopping Power

### 2.4.1. Definition of Stopping Power

Stopping power is defined as the average energy loss of the particle per unit path length. Unit of the stopping power is MeV/cm (Equation 2.2).

**S(E) = (dE/dx)** (Equation 2.2)

When charged ion enters and passes through matters, the ion travels until it loses all of its energies and takes a rest within matters. Incident ion stops the travel eventually since there is a certain amount of power of matters to resist against ion passage. During the passage, the ion experiences collisions with nuclei and electron clouds of target atoms. Due to the collisions, the incident ion transfers its kinetic energy to matters all the time. The ion comes to rest when the ion has no more energy to transfer its kinetic energy into target atoms and travel within matters. The lost of kinetic energy occurs gradually in steps. This process of rest of ion is so called stopping of ion in matters (Figure 2.20). Stopping power is equivalent to the power of matters to resist against ion passage [22].

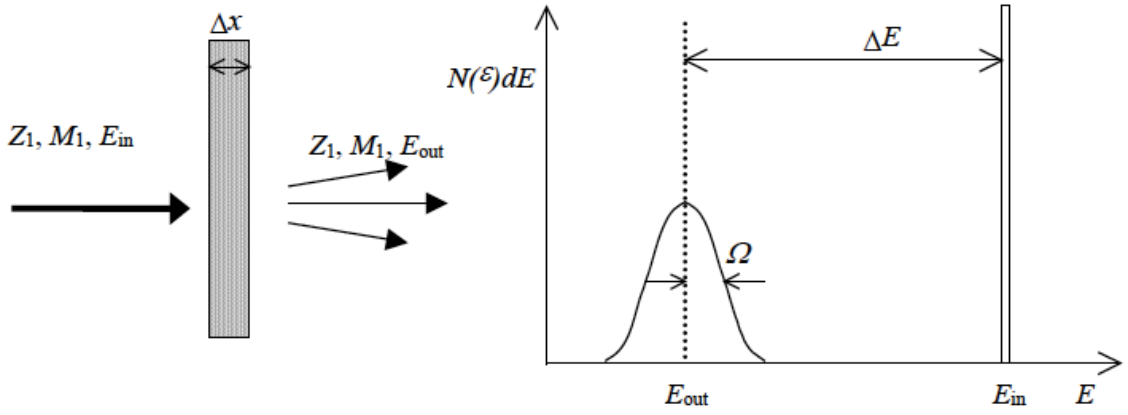


Figure 2.20. Stopping power and energy loss [23]

The stopping power consists of two parts; nuclear stopping and electronic stopping. The energetic ion collides with target atoms and loses its energy due to its nuclear energy loss process (Equation 2.3). At the same time the incident charged ion ionizes target atoms as the ion captures and loses electrons all the time while ion is passing through clouds of electrons surrounding nuclei of target atoms.

$$\mathbf{(dE/dx)_{total}} = (dE/dx)_{nuclear} + (dE/dx)_{electronic} \qquad \text{(Equation 2.3)}$$

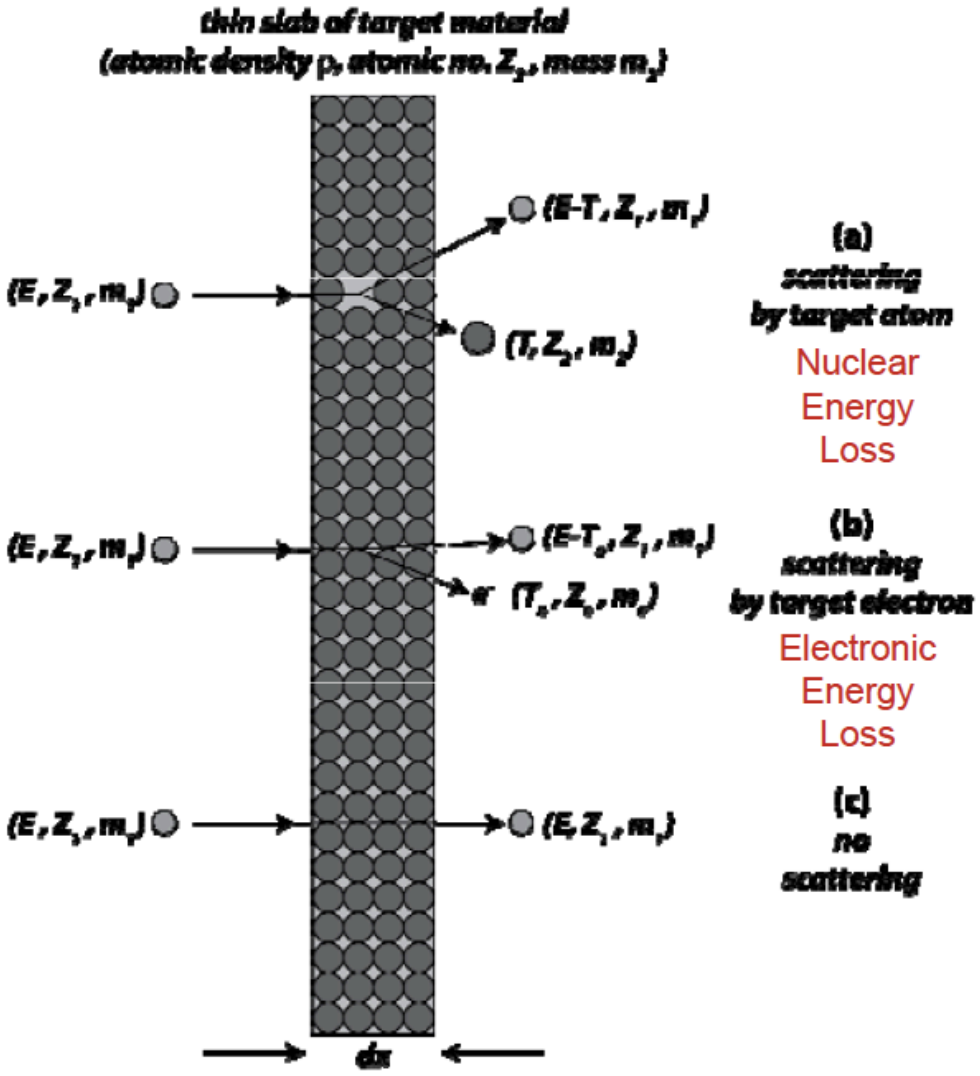


Figure 2.21. Partitioning of energy loss, dE/dx [23]

Nuclear energy loss occurs when nucleus of incident ion collides with nuclei of target atoms (Figure 2.22). The collisions can be described by energy and momentum conservation. The incident ion loses its energy as imparting its energy to target atoms while penetrating matters. Elastic collisions of screen coulomb type induce large ΔE, deflections, and damages to materials.

$(dE/dx)_{nuclear}$ = nuclear stopping power (Equation 2.4)

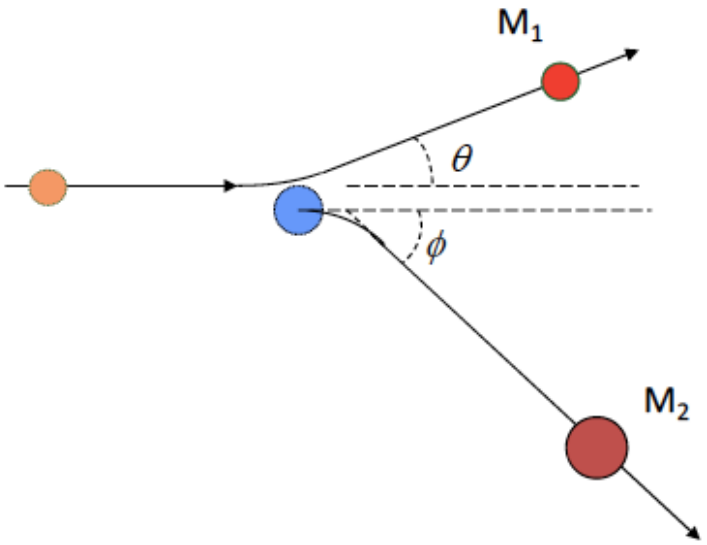


Figure 2.22. Nuclear energy loss [23]

Electronic energy loss occurs when electrons of incident ion collides with electrons of target atoms. The incident ion captures and loses electrons constantly while moving through a sea of electrons (Figure 2.23). Due to energy gain and loss to electrons, ionization and excitation are accompanied. Small ΔE and deflections are featured.

$(dE/dx)_{electronic}$ = electronic stopping power (Equation 2.5)

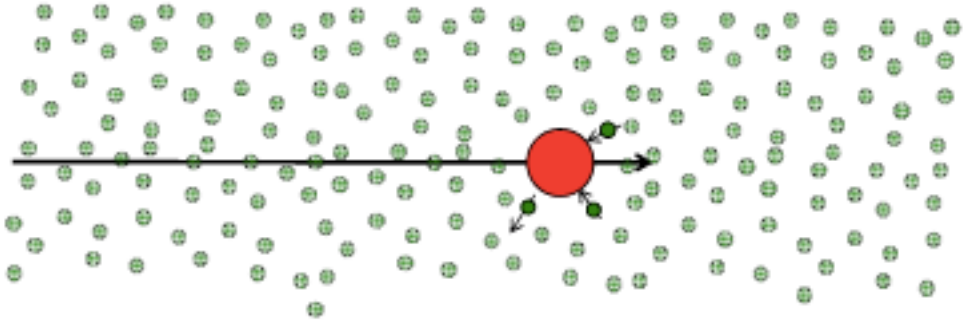

Figure 2.23. Electronic energy loss [23]

### 2.4.2. Importance of Stopping Power

Stopping power is an important parameter to estimate range of energetic particle within matters, size and shape of interaction volume, and efficiency of producing and discerning different signals. Projected range is defined as; the shortest distance between surface and the point where the ion comes to rest as incident ion enters matter and experience collisions with atoms of matter (Figure 2.24). Range of incident ion helps to understand lateral and depth distribution of energy deposited, so that we are able to figure out estimated geometric distribution and boundary where interactions with target atoms may occur in matters. This size and shape of interaction volume enables to estimate geometric map where secondary electrons are produced and emitted in matter, even further how many secondary electron yields will be produced with correct information of effective escape depth (λ) and secondary electron excitation energy (ε) of materials. For the upcoming Monte Carlo modeling of helium ion beam induced secondary electron yields, the simulation software incorporated with the 1$^{st}$ approximation of stopping power curve, universal ASTAR curve, will makes it possible to

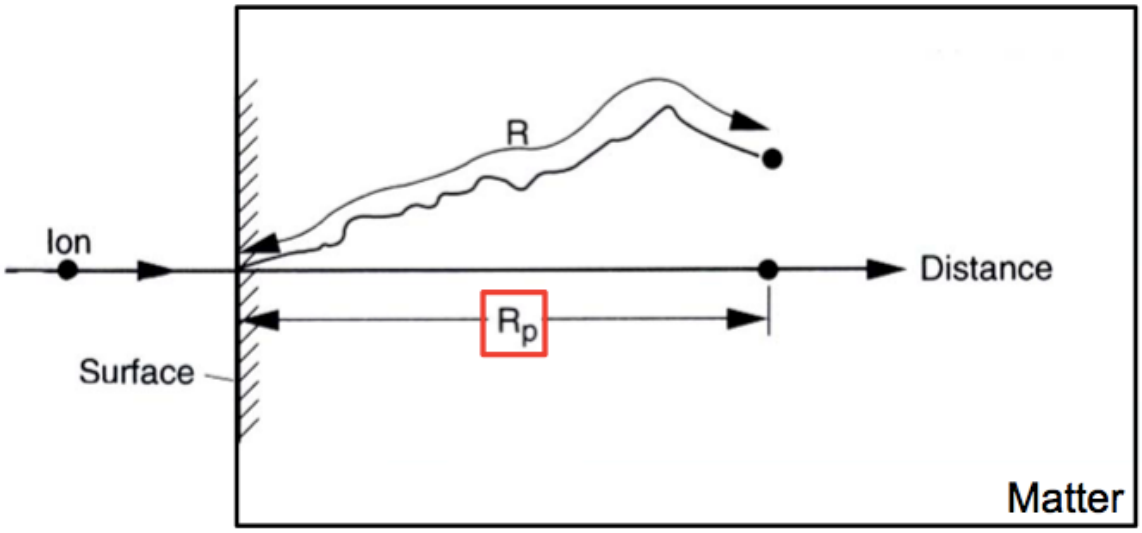


Figure 2.24. Description of projected range ($R_P$)

estimate the projected range of incident helium ion and consequently, predict the iSE yields-as a result of integrating the Bethe's theory and the probability of an electron escaping to an infinite planar surface from depth-for both pure elements and compounds in wide range of energies. Again, determining the appropriate values of stopping power is the first step to compute the iSE yield through the Monte Carlo simulation method.

# Chapter 3

# Modeling iSE Yield

## 3.1. Monte Carlo Modeling

Next generation Monte Carlo simulation software with use of universal ASTAR curve of helium stopping power as a function of energy will model helium ion induced secondary electron production within matters for both pure elements and compounds. The Monte Carlo Simulation Modeling in the current study adopted the fundamental framework of Monte Carlo simulation for the interaction of electron beam with a solid using the "single scattering" approximation [20]. However, certain amount of partial change was given to the simulation since interaction of ion beam with a solid has quite different features and even further, more complex natures than that of electron beam with a solid. In case of interaction of ion with a solid, the incident swift ion experiences both elastic and inelastic scattering within matter. When ion collides with nuclei of target atoms, kinetic energy and momentum of the system is conserved like collision of billiards ball, which is classified as the elastic scattering and where nuclear stopping power dominates the collision. While smaller energy losses are given during the elastic scattering event, significant amount of energy losses, during this inelastic scattering event, are experienced when the incident ion moves through a sea of electrons in a solid and undergoes collisions with the electrons; captures and loses electrons all the time. Ion loses its energy gradually and continuously through its passage through solid until the ion takes rest within solid.

With previously described intrinsic nature of both elastic and inelastic ion-matter interaction, modeling tracking down the propagation of the ion through the solid from one interaction to the next will be built on two assumptions to include the most essential parameters of the scattering events, so that necessary computation time could

be significantly reduced. Firstly, path of the ion will be determined by only elastic scattering events. The incident ion will experience Rutherford scattering events with high dependence on nuclear scattering cross sections of target atoms for the ions. Angular deflection of the ion ranges from 0° to 180°. Secondly, the electron propagation within solid loses its energy gradually and continuously through the passages by the Bethe relationship. In this inelastic scattering event, electronic stopping power plays key roll in the energy loss [24].

To model the ion beam induced secondary electron yield with the slightly revised "single scattering" approximation and the continuous-slowing-down (CSD) approximation among two of the simulation approaches [1], the current Monte Carlo simulation built on previously stated two approximations will trace each ion trajectories in matters. With effort to calculate the projected range of ion, the probability of iSE produced at certain depth (x) in the matter should be able to be computed. The probability and the ion stopping power of material, electronic stopping power to be more specific, will be put in an equation to evaluate the Monte Carlo simulation of the SE yield, which contributes to ten-times-faster computation time with equal simulation results. In order to predict the projected range of ion, there must be clearly clarified basic sequence of prediction of the ion trajectory at each step. Computing the probability incorporated with the stopping power will be a completion of a loop to predict number of secondary electrons produced by each incident ion beam. Consequently, a sequence of Monte Carlo modeling is organized referring to previous studies [20, 25] as below.

Projected range of ion could be estimated when all the trajectories of ions are traced and lateral distribution of the ion location is computed. While simulating the propagation of ion within solid, the geometry of ion trajectory in Figure 3.1 shows the ion experiences elastic scattering events, so that the ion moves from a certain point (where ion interaction with atom occurs), $P_n$ ($x_n$, $y_n$, $z_n$) to the next point, $P_{n+1}$ ($x_{n+!}$, $y_{n+!}$,

$z_{n+1}$), with change in its energy, dE/dS, and direction of ion propagation, scattering angle θ & azimuthal deflection ϕ. This unit path could be extended forward to the propagation direction, from $P_{n+1}$ ($x_{n+1}$, $y_{n+1}$, $z_{n+1}$) to $P_{n+2}$ ($x_{n+2}$, $y_{n+2}$, $z_{n+2}$), or extend backward, from $P_n$ ($x_n$, $y_n$, $z_n$) to $P_{n-1}$ ($x_{n-1}$, $y_{n-1}$, $z_{n-1}$). These extension of the ion path will be stretched forward to the end point of ion motion, where ion takes rest after losing all energies, and backward to the start point of ion interaction with matter. A trajectory is completed as a result of including all the paths of ion propagation from the start to the end point. Another trajectory will be initiated immediately as soon as another ion is bombarded to the solid. To determine the energy loss, dE/dS, of ion in motion as it travels along this unit path, two significant parameters also needs to be determined; firstly, residual energy, $E_n$, of ion at certain point, $P_n$ ($x_n$, $y_n$, $z_n$), secondly, length of each path, S between its successive last and next events. The above computation of ion trajectory, ion interaction with solid, is only valid when the ion is located within the specimen. So, the location of the ion needs to be frequently checked if the ion is outside the surface of solid or its energy is below 250 eV. If this is the case then this trajectory is terminated and a new trajectory is initiated from the initial entry coordinates and energy of incident ion. Otherwise this loop is repeated until the ion loses all of its energies. The loop will be finished up as tracing all the trajectories are complete as all the incident ions experience the ion-solid interactions. With completion of the loop, total path length, projected range, could be derived. Total secondary electron yield will be calculated, with projected range incorporated into the formula, by integrating the ion stopping power for the material and the probability of an electron escaping to a planar surface from depth z.

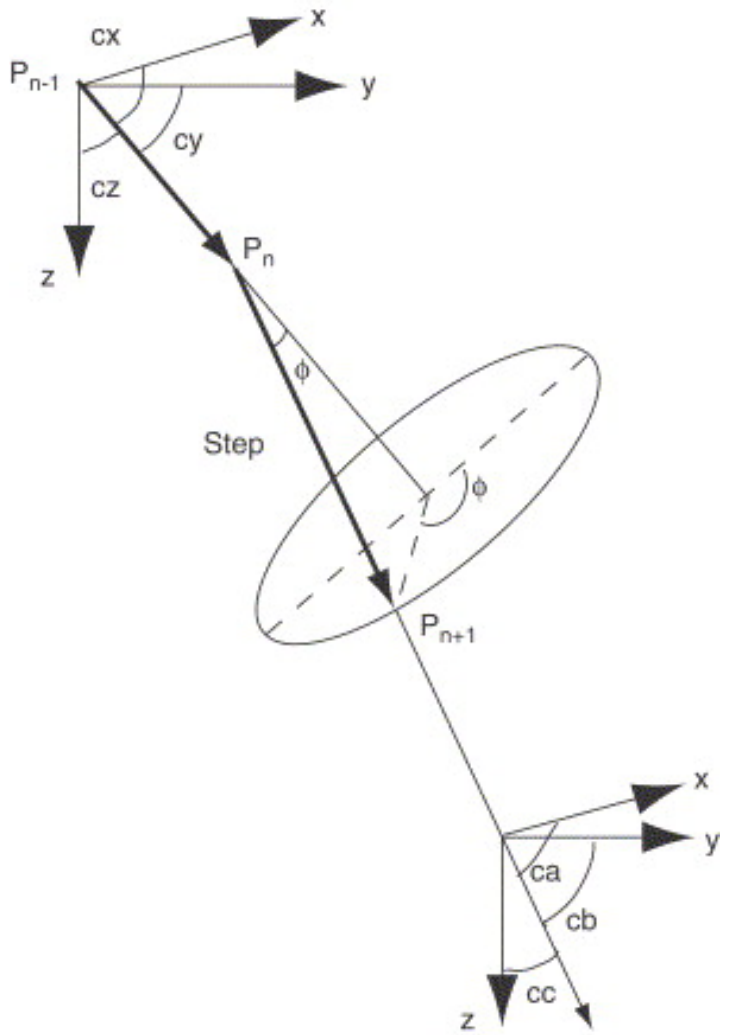


Figure 3.1. Definition of coordinate system used in the Monte Carlo simulation program [20]

### 3.2. Parameter Input & Details of Physics

#### 3.2.1. Incident Ion

The scattering angle θ is calculated from simple analytical evaluation of the scattering angle optimized for low ion energies suggested by Biersack and Haggmark [26]. The scattering angle is evaluated by repulsive interaction between incident particle of mass $M_1$ having kinetic energy E and stationary particle of mass $M_2$ in the center-of-mass (CM) system (Figure 3.2) as

$$\cos(\theta/2) = (\rho + P + \delta) / (\rho + r_0) \qquad \text{(Equation 3.1)}$$

$$\rho = \rho_1 + \rho_2$$
$$\delta = \delta_1 + \delta_2$$

where $\rho_1$, $\rho_2$ are radii of curvature of the trajectories at closest approach, $\delta_1 + \delta_2$ are correction terms and P, $r_0$ are impact parameter and distance of closest approach respectively, which are known values.

The distance of closest approach $r_0$ is given from below equation

$$1 - V(r_0) / E_c - (P/r_0)^2 = 0 \qquad \text{(Equation 3.2)}$$

where $E_c = E / (1 + M_1/M_2)$ is the energy available in the center-of-mass system and V(r) is the interaction potential between the incident ion and the target atom.

Radii of curvature of the trajectories at closest approach is evaluated as correlating particles' mass, velocity, and centrifugal force, $f_c$, with ρ

$$\rho = \rho_1 + \rho_2 = (M_1 v_1^2 + M_2 v_2^2) / f_c \qquad \text{(Equation 3.3)}$$

as kinetic energy and force are expressed in terms of Ec and V, ρ could be written

$$\rho = -2 (E_c - V(r_0)) / V'(r_0) \qquad \text{(Equation 3.4)}$$

where $V'(r_0)$ is the spatial derivative of the potential evaluated at $r_o$.

The dimensionless reduced energy, ε, is introduced

$$\varepsilon = a E_c / (Z_1 Z_2 e^2) \qquad \text{(Equation 3.5)}$$

where $Z_1$ and $Z_2$ are the incident particle and target atomic numbers, respectively, e and a are the electronic charge, and the screening length respectively.

For choosing the right screening length, Firsov screening length [27] is picked up

$$a = 0.8853 a_0 / (Z_1^{1/2} + Z_2^{1/2})^{2/3} \qquad \text{(Equation 3.6)}$$

where $a_0 = 0.529$ Å is the Bohr radius. To express the scattering angle, θ, with the equation, ρ, P, δ, and $r_0$ are defined as below

$$\rho = a R_c, \quad P = a B, \quad \delta = a \Delta, \quad \text{and } r_0 = a R_0$$

cos(θ/2) is derived when ρ, P, δ, and $r_0$ are put into equation

$$\cos(\theta/2) = (B + R_c + \Delta) / (R_0 + R_c) \qquad \text{(Equation 3.7)}$$

which gives

$$\theta = 2\cos^{-1}((B + R_c + \Delta) / (R_0 + R_c)) \qquad \text{(Equation 3.8)}$$

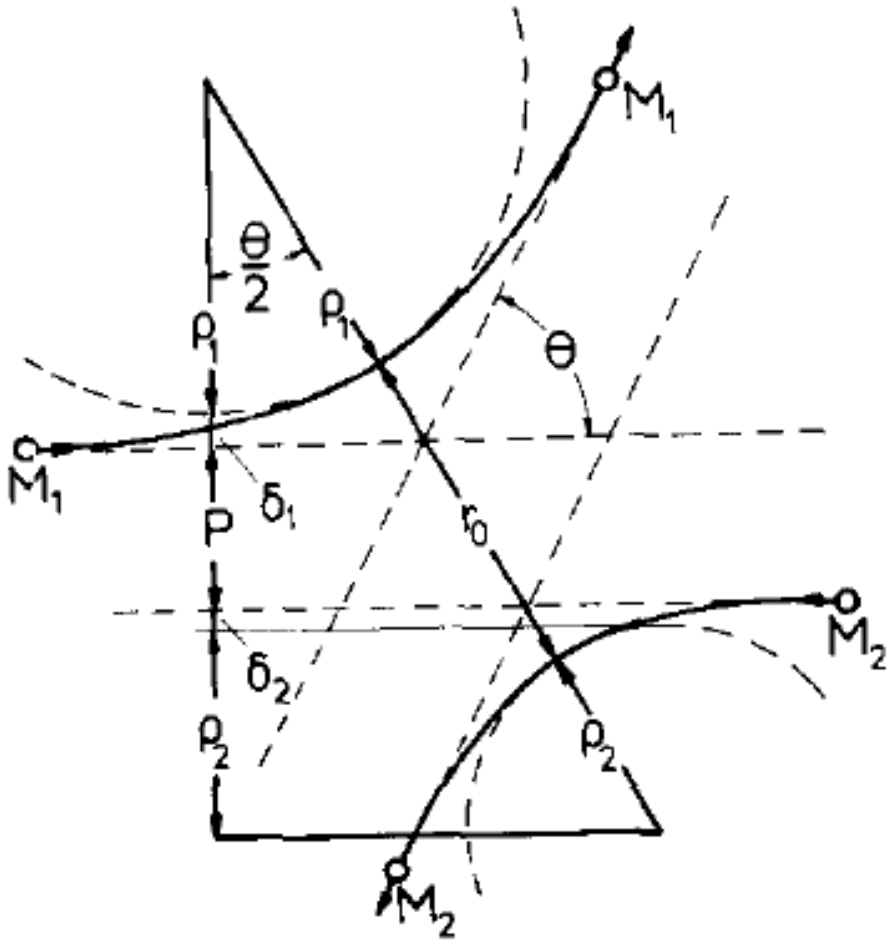


Figure 3.2. The particle trajectories in the center-of-mass (CM) system with superimposed "scattering triangle," comprised of impact parameter P, radii of curvature $\rho_1$ and $\rho_2$, distance of closest approach $r_0$, and the correction terms $\delta_1$ and $\delta_2$. From this construction $\cos(\theta/2)$ is obtained [26].

The azimuthal scattering angle $\phi$ is $2\pi$ RND where RND is a random number between 0 and 1.

The mean free path, $\lambda$, is calculated from comprehensive integration of individual work of the Lindhard, Nielson, Scharff differential cross-section $d\sigma(E,T)$, the universal screening radius a, fitting LNS $f(t^{1/2})$ [28-31]

$$\lambda = M_2 / (N_a \rho \sigma_T) \quad \text{(Equation 3.9)}$$

where $N_a$ is the Avogadro's number, $\rho$ is the density of the target, $\sigma_T$ is the total cross section. The distance of ion traveling when the mean free path is $\lambda$ is

$$S = - \lambda \log_e(RND) \quad \text{(Equation 3.10)}$$

where RND is a random number between 0 and 1.

The nuclear energy loss is calculated as

$$(\Delta E)_{nuclear} = 4M_1M_2 / (M_1 + M_2)^2 \sin^2(\theta/2) E \quad \text{(Equation 3.11)}$$

The electronic energy loss is calculated as

$$(\Delta E)_{electronic} = S(dE/dS)_{Helium\ Electronic} = S (4\gamma^2_{He} (dE/dS)_{Proton\ Electronic}) \quad \text{(Equation 3.12)}$$

where $\gamma_{He}$ is the fractional effective charge of the helium ion.

For faster calculation using the Monte Carlo simulation technique with reduced number of physical parameters, it is assumed that the density of the target stays constant.

### 3.2.2. Secondary Electrons

The current approach used here, to model ion beam induced secondary electron, is based on referring to and integration of the previous works (theoretical model for iSE production, first principles calculations, and developments) proposed and consolidated by many others [32-37].

Bethe [38] proposed the idea that the secondary electron emission from solid is proportional to the ratio of the rates of energy loss (stopping power) of incident particle in solid. This is, through experiment, demonstrated by large number of SE production by protons in metal and insulators. The Bethe's theory is later proven to be valid for the case of iSE generation by both electron and ion incident beam by Scheifein and others [39].

$$\delta_{SE} = -(1/\varepsilon)(dE/dS) \qquad \text{(Equation 3.13)}$$

where $\delta_{SE}$ is the SE yield, dE/dS is the stopping power (eV/A) along the trajectory of the particle, and ε is a scaling constant. For input of the stopping power, dE/dS will be replaced with $(dE/dS)_{electronic}$ since electronic stopping power is proposed to play major role in production of iSE and weight of nuclear stopping power to the total stopping power is negligible when helium ion interacts with solid at the velocities of interest [37, 40].

Salow [41] proposed the idea that iSE escapes from a solid by diffusion process, so that the probability, p(z), of an electron escaping to an infinite planar surface from depth z is evaluated as

$$p(z) = A \exp(-z/\lambda) \qquad \text{(Equation 3.14)}$$

where z is depth from infinite planar surface, $\lambda_d$ is the effective diffusion length for the secondary electron and A is a scaling constant. Integration of equation & gives rise to the total secondary electron yield, $\delta_{SE}$

$$\delta_{SE} = \int_0^R \frac{dE}{dz} 0.5 \exp(-z/\lambda d) dz \quad \text{(Equation 3.15)}$$

where R is the projected range of the incident particle.

### 3.2.3. Random Number Generation

The generated random number, $x, \forall x \in (0,1),$ are uniformly distributed by Equation 3.16 and generated as shown in Algorithm 1. C++ uses the linear congruential method for random-number generation in the RND function. The linear congruential method has an advantage of requiring only a few operations per call, so that computation is significantly fast. However, constants of multiplier, increment, and modulus are carefully to be chosen to have sequential correlation on successive calls [42]. The 'MOD' operator in the formula below returns the integer remainder after an integer division. The expression x1/(2^24) will then return the floating-point number between 0.0 and 1.0 that is returned by the RND function.

x1 = ( x0 * a + c ) MOD (2^24) (Equation 3.16)

where

x1 = new value

x0 = previous value

a = 1140671485 (multiplier)

c = 12820163 (increment)

2^24 (modulus)

Note that, by default, the Rnd() function will return the same sequence of pseudo-random numbers each time the program is run. For some purposes (such as statistical studies where repeatability is required) this may be appropriate. For other types of applications, such as games, this may not be appropriate. The notation '&' in Algorithm 1 stands for 'AND bitwise operator' as 1000 & 1111 = 1000, 1100 & 0011 = 0000, 1010 & 1010 = 1010 [43].

```
Variable := x, a
a ← Call time(0)
Call srand(b)
x ← Call Rnd()

function Rnd()
{
    Variable := b, c, d
        b ← Call rand()
        c ← (b * 1140671485 + 12820163) & 16777215
        d ← c / (2^24)
    return d;
}
```

Algorithm 1. srand, time, and rand functions are provided by standard c++ library.

### 3.2.4. Visualization of Results

The Monte Carlo Simulation is implemented by $C^{++}$ and tested on Windows 7 operating system. With an attempt to calculate the projected range, paths of each ion trajectories are illustrated graphically indicating the vertical and lateral range of ion-solid interaction, so called interaction volume. The IONiSE software (the Monte Carlo Simulation program) makes it possible to visualize the propagation of ions with adoption of different colors corresponding to change in depth from the planar surface, for example, the trajectory is expressed with blue color from the surface to 100 nm deep and shown with red from 100 nm to 200 nm deep and so on. This graphical variation is aimed to give immediate intuitive estimation of length of paths. This graphical description of ion-solid interaction behavior results in obtaining the projected range to calculate the iSE yield over ion beam range from 10 keV to 100 keV, where effective range of ion beam in use and $1^{st}$ approximation of the universal stopping power curve for he ion incorporated. The iSE yield, projected range, and backscattered ion yield is obtained as numerical values with two decimal point accuracy as well as the graphical description of ion-solid interaction. To obtain ion beam induced secondary electron yields, there are three options to choose incident ions among H, He, and Ga, which are to be believed appropriate source of ion for ion microscope. For calculation of any certain ion beam induced secondary electron yields, choice of materials-both pure element and compounds-need to be performed concurrently. Calculation of iSE yield for compound materials requires careful input of stoichiometry of the solid.

# Chapter 4

# Results and Discussion

## 4.1. Results

### 4.1.1. iSE Yields for Pure Elements

The IONiSE has been applied to calculate helium ion beam induced secondary electron yield, projected range, and backscattered ion yield over ion beam range from 10 keV to 100 keV. 40 keV is default for energy of incident ion beam. Silicon as solid-pure element- is default material and number of generation of random number is set 1,000, defaults, for fast computation time. The input of random number ranges from 1,000 and 100,00. The estimated range is calculated with visualization of ion trajectories in different colors with depths. The projected range is estimated and this value will be used to calculate the helium ion beam induced secondary electron yield. The computed SE yield could be divided into $SE_1$ and $SE_2$ yield. For solid, silicon, iron and gold are chosen since there are basic and the most fundamental materials in semiconductor industry and nano-science. With choice of target material (Si, Fe, and Au), iSE yield is simulated and reported as 1.24, 4.72, and 7.93, respectively while projected range is reduced 560 nm, 270 nm, and 160 nm, respectively. It is obvious that there is increase in iSE yield as increase in atomic number of target atom when incident ion, helium ion, remains constant. In the same fashion, backscattered ion yield for helium ion is reported 0.10 %, 1.30 %, and 2.80 %, respectively in accordance with increase in atomic number of target atom (Figure 4.1, 4.2, and 4.3). These changes in iSE yield and projected range indicate target atom with higher atomic number produces shorter projected range, accompanying larger number of iSE yield and higher number of backscattered ion yield. These results are tabulated as table 4.1. These results will be more accurate with increase in number of generation of random number.

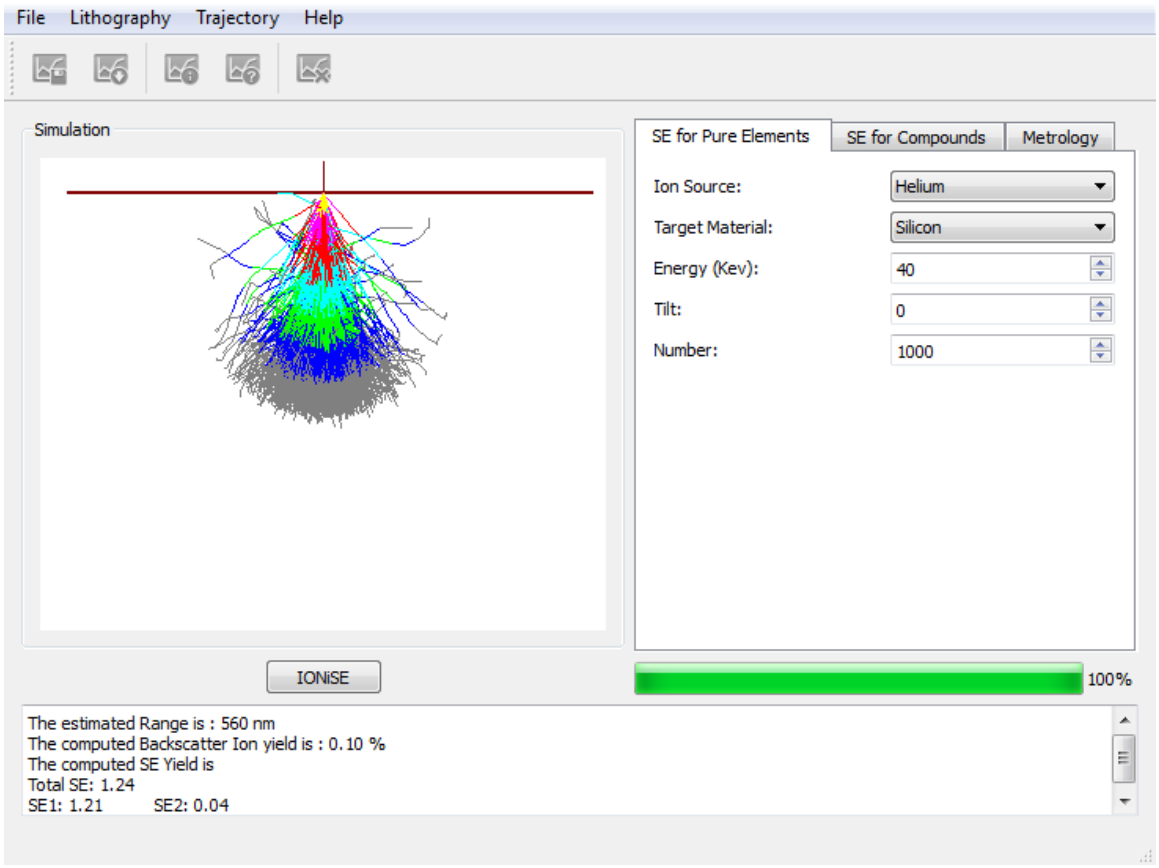


Figure 4.1. Monte Carlo simulation result of helium ion beam induced secondary electron yields of silicon

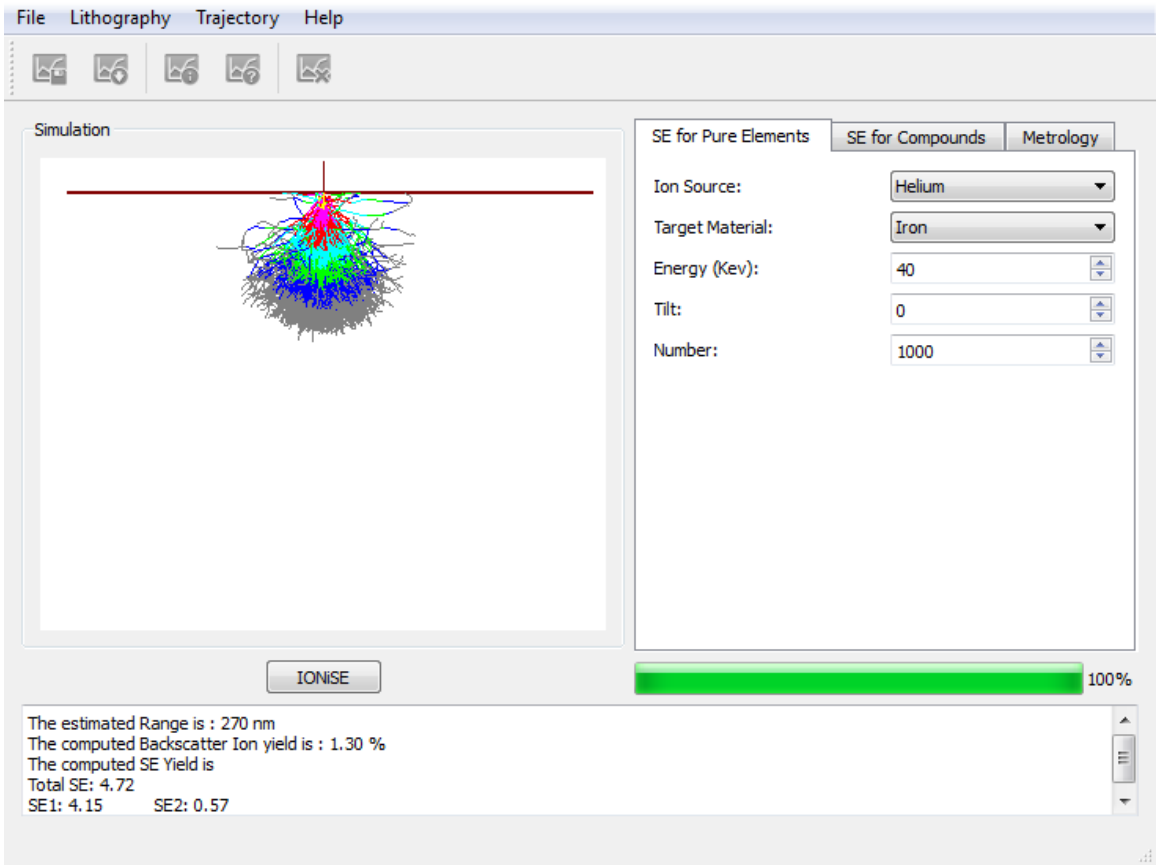


Figure 4.2. Monte Carlo simulation result of helium ion beam induced secondary electron yields of iron

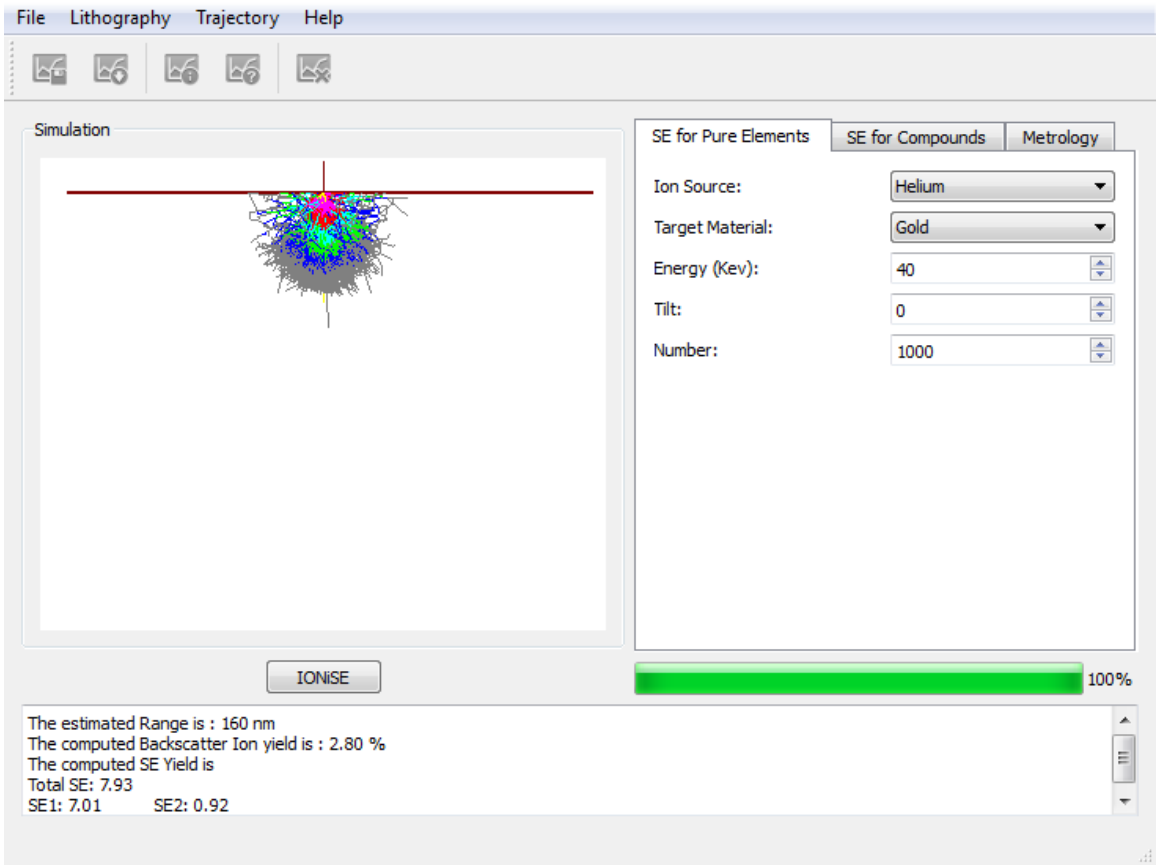


Figure 4.3. Monte Carlo simulation result of helium ion beam induced secondary electron yields of gold

Table 4.1. IONiSE aided-simulated iSE yield, projected range, and backscattered yield values of incident helium ion beam for pure elements

| Incident Ion | Helium (40 keV) | iSE Yield | $R_P$ (nm) | Backscattered Ion Yield (%) |
|---|---|---|---|---|
| Solid | Si (At. #: 14) | 1.24 | 560 | 0.10 |
| | Fe (At. #: 26) | 4.72 | 270 | 1.30 |
| | Au (At. #: 79) | 7.93 | 160 | 2.80 |

### 4.1.2. iSE Yields for Compounds

This will be the most interesting and important part of computation to calculate the iSE yield results given by the idea incorporating the universal ASTAR curve of stopping power into the IONiSE software, which was not available before. The helium ion beam induced secondary electron yield, projected range, and backscattered ion yield over ion beam range from 10 keV to 100 keV are computed and tabulated in Table 4.2. 40 keV is default for energy of incident ion beam and number of generation of random number is set 1,000, default, for fast computation time. The input of random number ranges from 1,000 and 100,00. For solid, the most popular contemporary compound materials, silicon carbide, gallium nitride, gallium arsenide, molybdenum disulfide, indium phosphide, and gallium antimonide are chosen. With choice of target material (SiC, GaN, $MoS_2$, InP, and GaSb), iSE yield is simulated and reported as 0.26, 0.18, 0.36, 0.46, 0.77, and 0.91, respectively while projected range is reported 570 nm, 1,070 nm, 330 nm, 600 nm, 650 nm and 300 nm, respectively. Backscattered ion yield for helium ion is reported 0.20 %, 1.20 %, 5.40 %, 3.20 %, 5.10 %, and 9.90 %, respectively (Figure 4.4, 4.5, 4.6, 4.7 and 4.8). These results are tabulated as table 4.2. These results will be more accurate with increase in number of generation of random number. Not like the case of pure element, it is hard to discuss any tendency since different stoichiometry of compounds has been introduced.

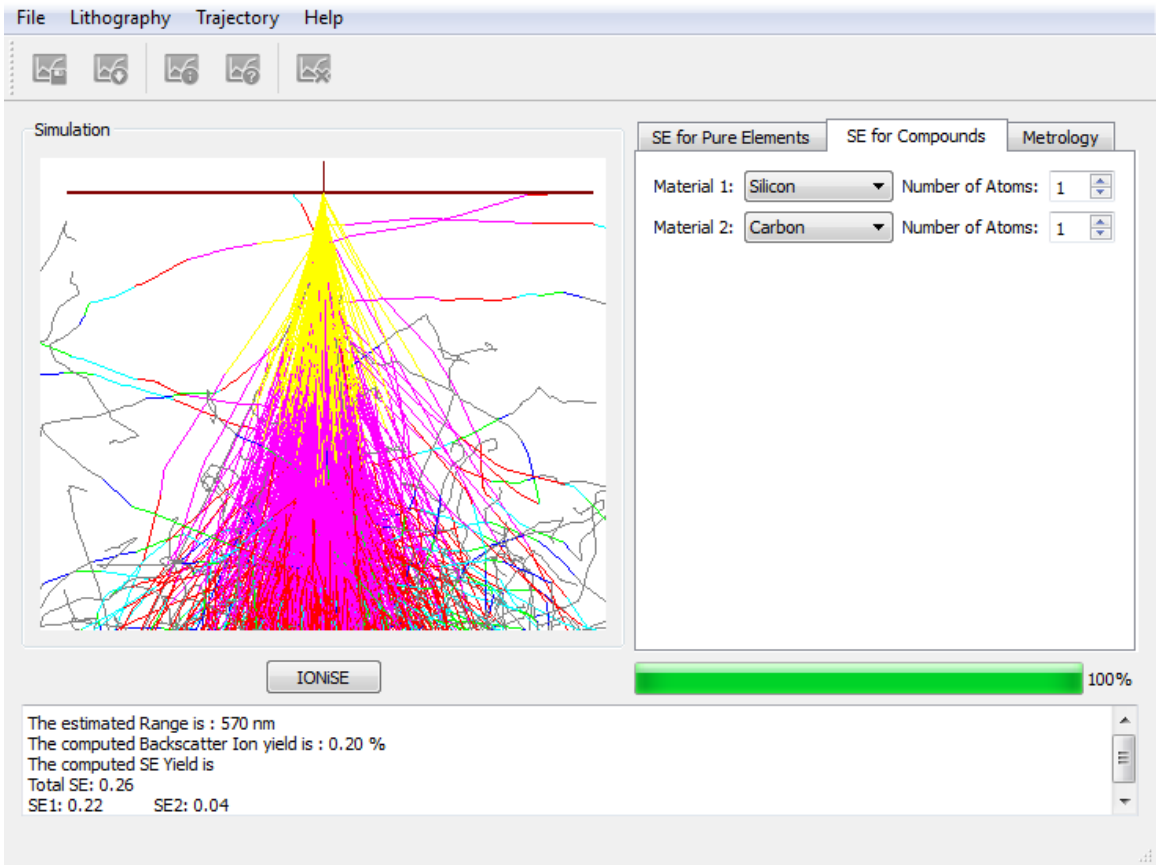


Figure 4.4. Monte Carlo simulation result of helium ion beam induced secondary electron yields of SiC

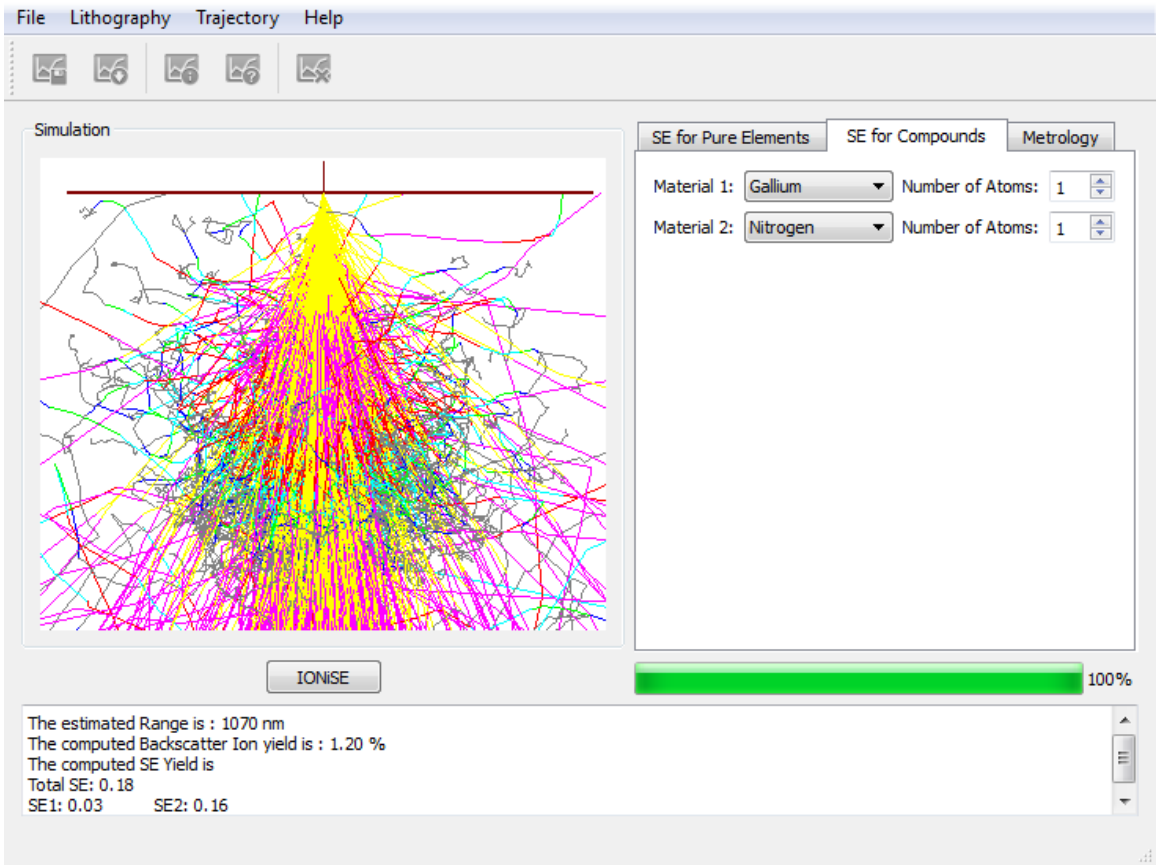


Figure 4.5. Monte Carlo simulation result of helium ion beam induced secondary electron yields of GaN

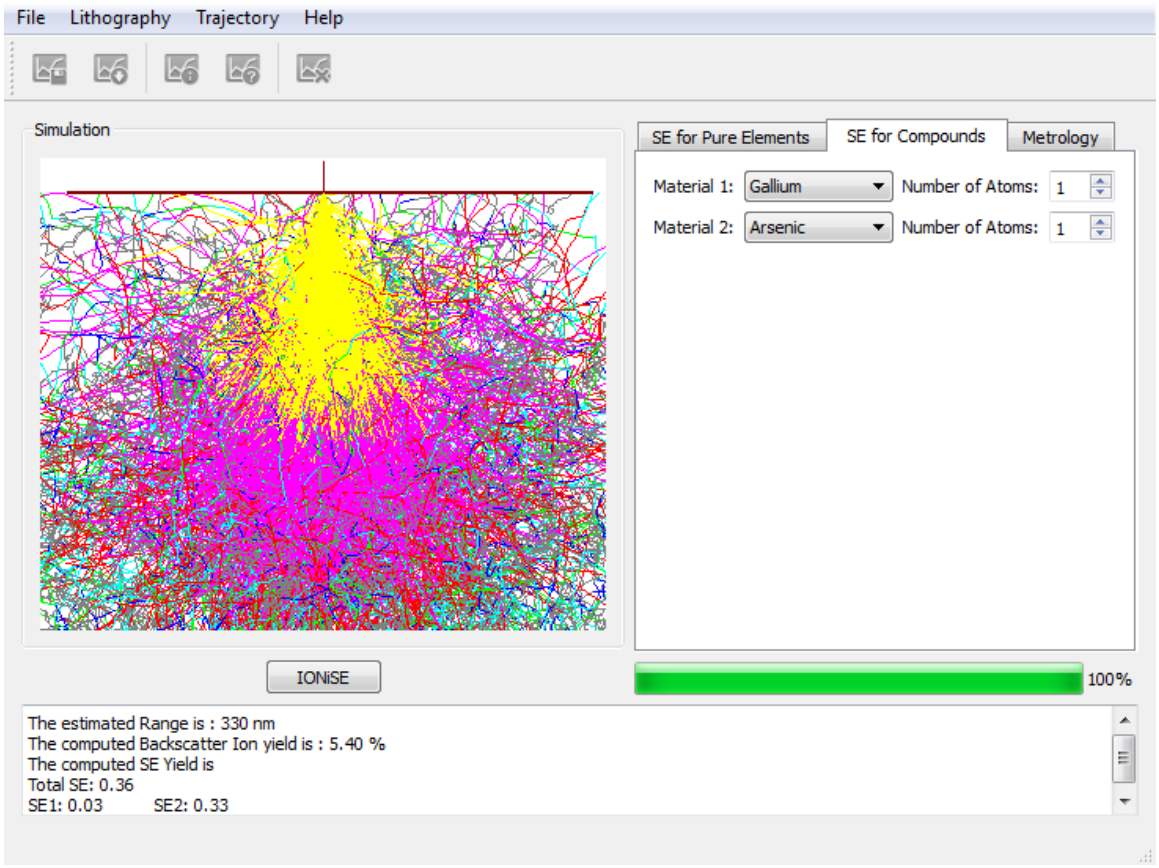


Figure 4.6. Monte Carlo simulation result of helium ion beam induced secondary electron yields of GaAs

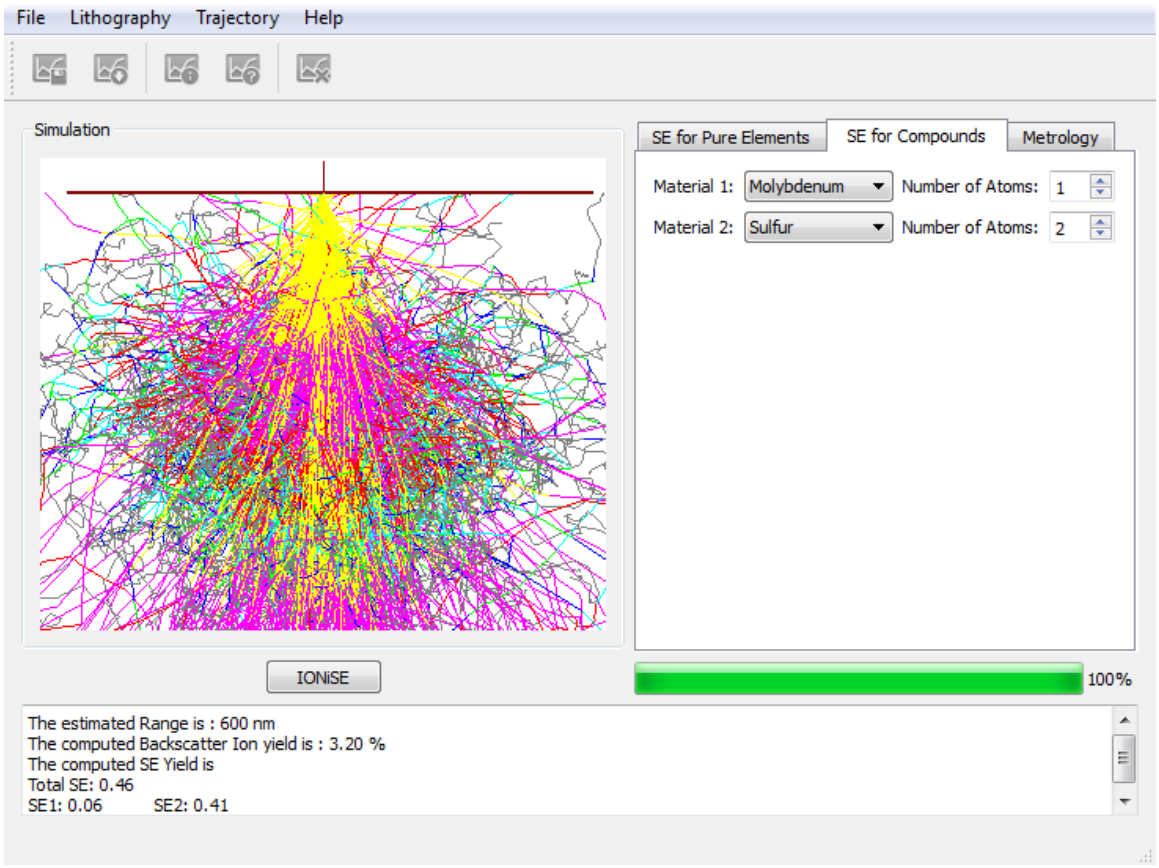


Figure 4.7. Monte Carlo simulation result of helium ion beam induced secondary electron yields of $MoS_2$

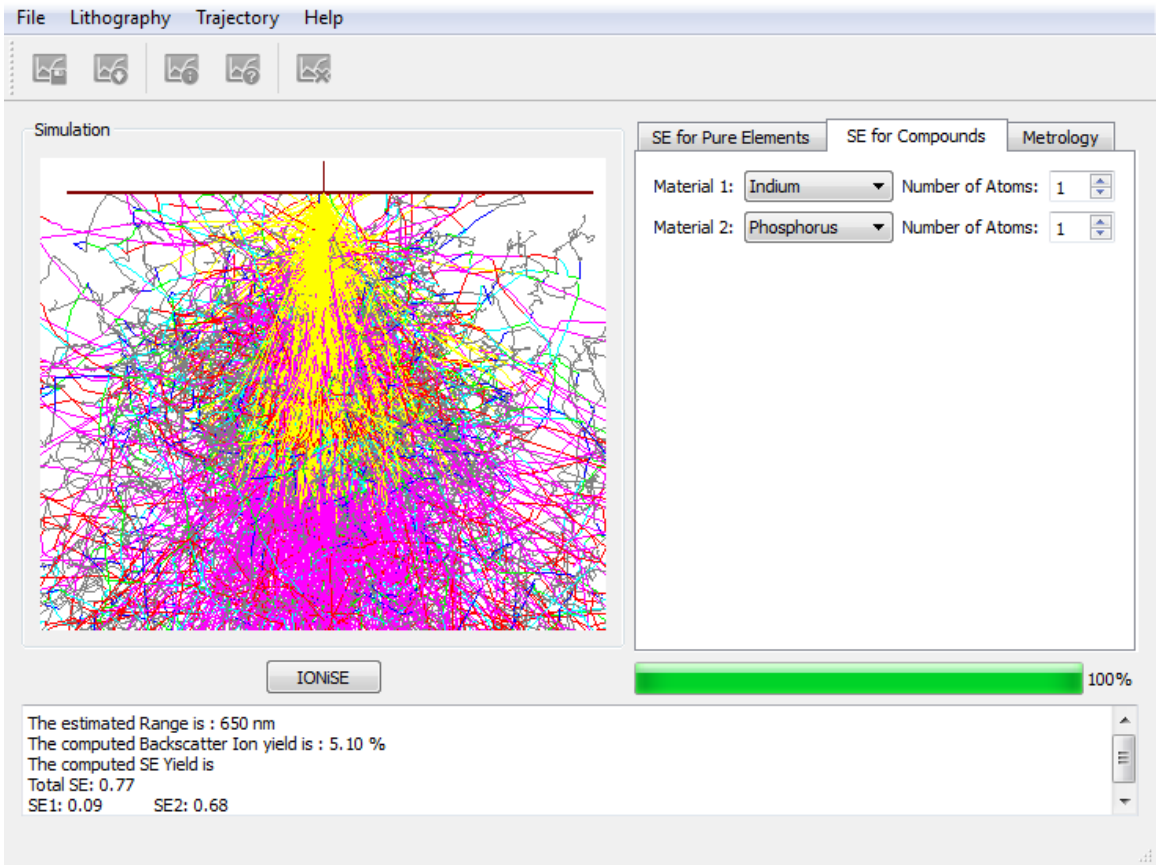


Figure 4.8. Monte Carlo simulation result of helium ion beam induced secondary electron yields of InP

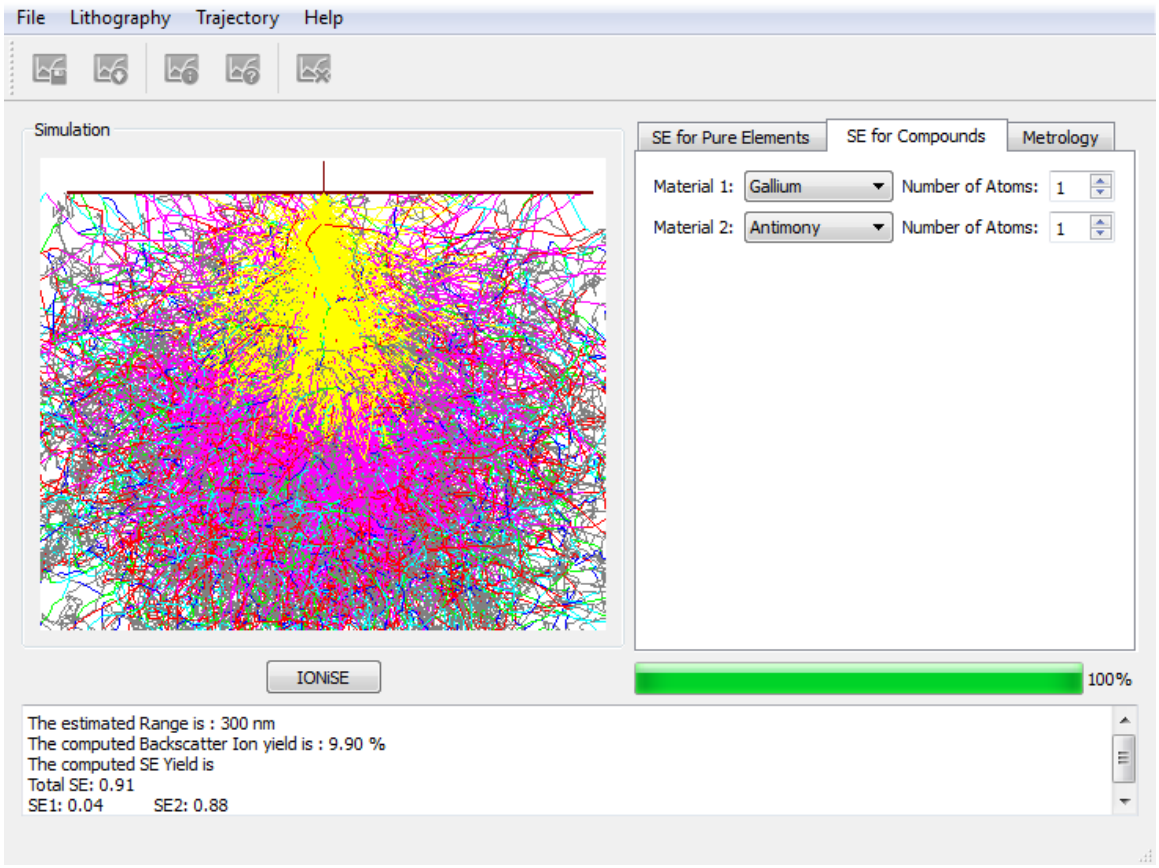


Figure 4.9. Monte Carlo simulation result of helium ion beam induced secondary electron yields of GaSb

Table 4.2. IONiSE aided-simulated iSE yield, projected range, and backscattered yield values of incident helium ion beam for compounds

| Incident Ion | Helium (40 keV) | iSE Yield | $R_P$ (nm) | Backscattered Ion Yield (%) |
|---|---|---|---|---|
| Compound | SiC | 0.26 | 570 | 0.20 |
| | GaN | 0.18 | 1,070 | 1.20 |
| | GaAs | 0.36 | 330 | 5.40 |
| | $MoS_2$ | 0.46 | 600 | 3.20 |
| | InP | 0.77 | 650 | 5.10 |
| | GaSb | 0.91 | 300 | 9.90 |

### 4.1.3. Critical Dimension Metrology

#### 4.1.3.1. Deposited Nano-Scale Lines

Line profiles are calculated with a topographic contrast, nano-sized bump, to measure line edge. This bump is equivalent to the case of deposited nano-scale line in semiconductor structures in the range of sub 50 nm. With advent of nano-sized structures smaller than electron beam interaction volume the development of critical dimension metrology enabled by the helium ion microscope has been at the center of

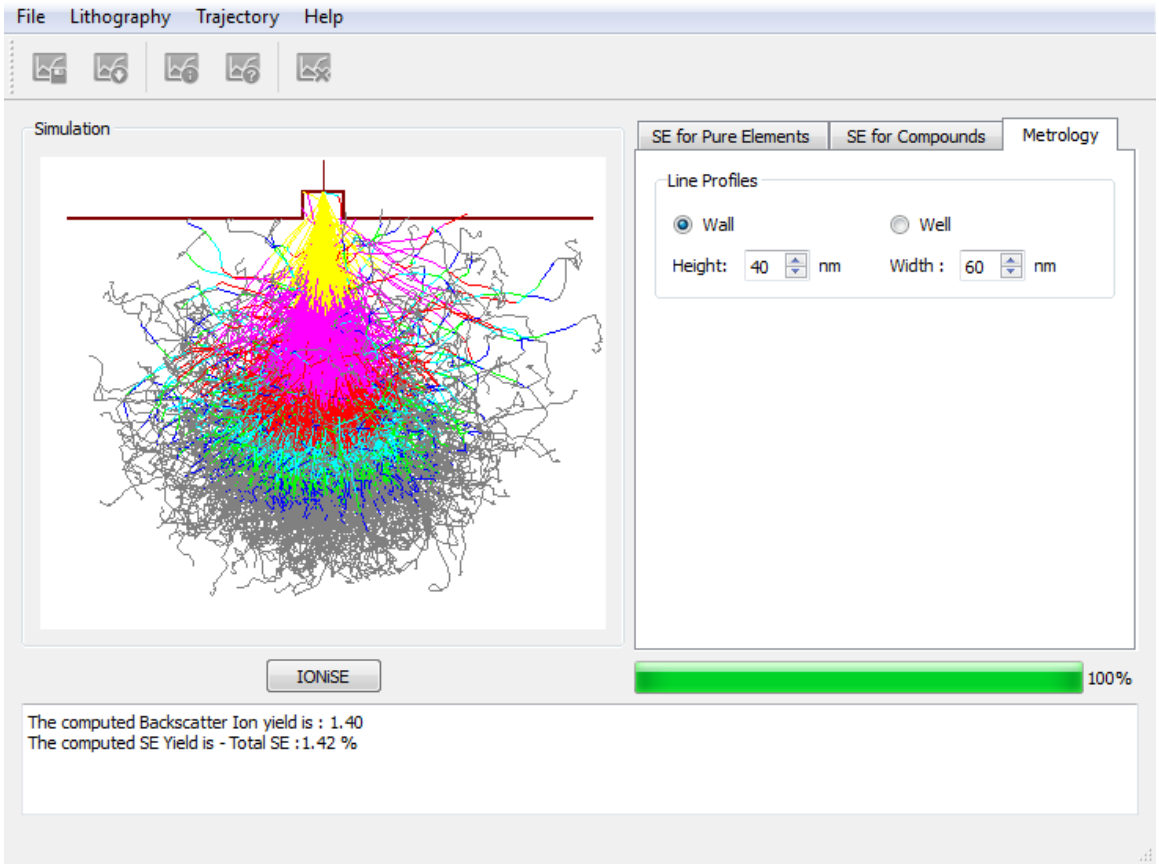


Figure 4.10. Monte Carlo simulation result of helium ion beam induced secondary electron yields of Si

interest in the field of semiconductor manufacturing. Hereby, the secondary electron yield is computed with topographical change, for example, deposited nano-scale lines (Figure 4.10) and etched nano-scale lines (Figure 4.11). The IONiSE has been applied to calculate helium ion beam induced secondary electron yield over ion beam range from 10 keV to 100 keV. 40 keV is default for energy of incident helium ion beam. Silicon as solid-pure element- is default material and number of generation of random number is set 1,000, defaults, for fast computation time. The input of random number ranges from 1,000 and 100,00. With the same lateral and vertical dimension of lengths (vertically 40 nm and horizontally 60 nm), protruded topographic structure gives rise to slightly higher secondary electron yield (from 1.39% to 1.42 %) and of course, larger backscattered ion yield (from 0.80% to 1.40 %) than flat surfaced-structure does as slightly closer surface to detector may result in this increase.

#### 4.1.3.2. Etched Nano-Scale Lines

Line profiles are calculated with a topographic contrast, nano-sized hall, to measure line edge. This hall is equivalent to the case of etched nano-scale line in semiconductor structures in the range of sub 50 nm. The IONiSE computed and predicted the helium ion beam induced secondary electron yield with topographical change, etched nano-scale lines, over ion beam range from 10 keV to 100 keV. The secondary electron yields and backscattered ion yield from the etched hall structure would be compared with those from the flat surfaced structures and protrudes structures as done in Figure 4.10.

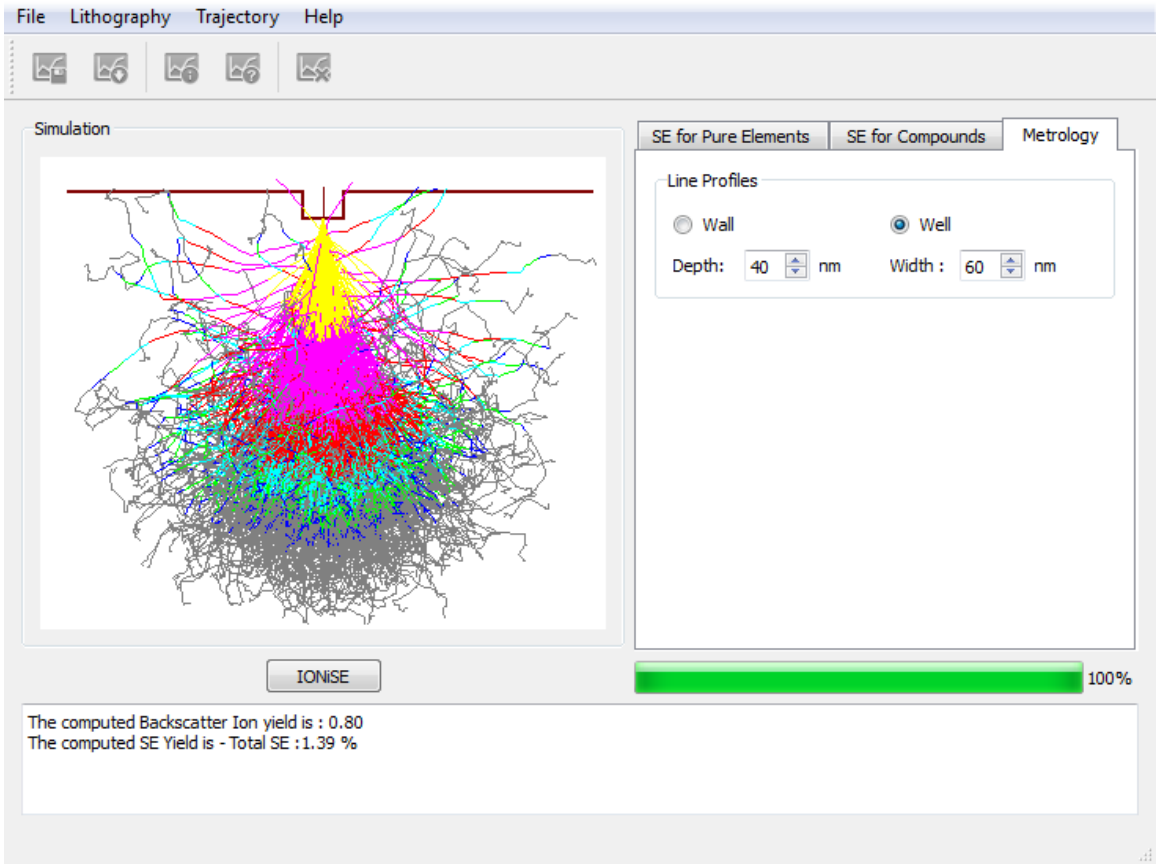


Figure 4.11. Monte Carlo simulation result of helium ion beam induced secondary electron yields of Si

**4.2. Discussion**

Table 4.1 indicates correlation of iSE yield, projected range of helium ion, and backscattered helium ion yield with atomic number. As atomic number increases twice (from Si (14) to Fe (26)), four times increase in iSE yield is calculated and demonstrated. However, there is twice increase in iSE yield when atomic number increases three times (from Fe (26) to Au (79) (Figure 4.12). This shows the rate of increase in iSE yield seems to be saturated as the atomic number approaches higher values. In close accordance with iSE yield, the rate of decrease in the projected range seems to be saturated as increase in atomic number as well. As atomic number increases twice (from Si (14) to Fe (26)), the projected range decreases roughly half. In similar result with the iSE yield behavior with atomic number, the range decreases about half as increase in atomic number three times (from Fe (26) to Au (79) (Figure 4.13). Backscattered ion yield behavior follows similar tendency of the iSE yield (Figure 4.14).

Table 4.1. IONiSE aided-simulated iSE yield, projected range, and backscattered yield values of incident helium ion beam for pure elements

| Incident Ion | Helium (40 keV) | iSE Yield | $R_P$ (nm) | Backscattered Ion Yield (%) |
|---|---|---|---|---|
| Solid | Si (At. #: 14) | 1.24 | 560 | 0.10 |
| | Fe (At. #: 26) | 4.72 | 270 | 1.30 |
| | Au (At. #: 79) | 7.93 | 160 | 2.80 |

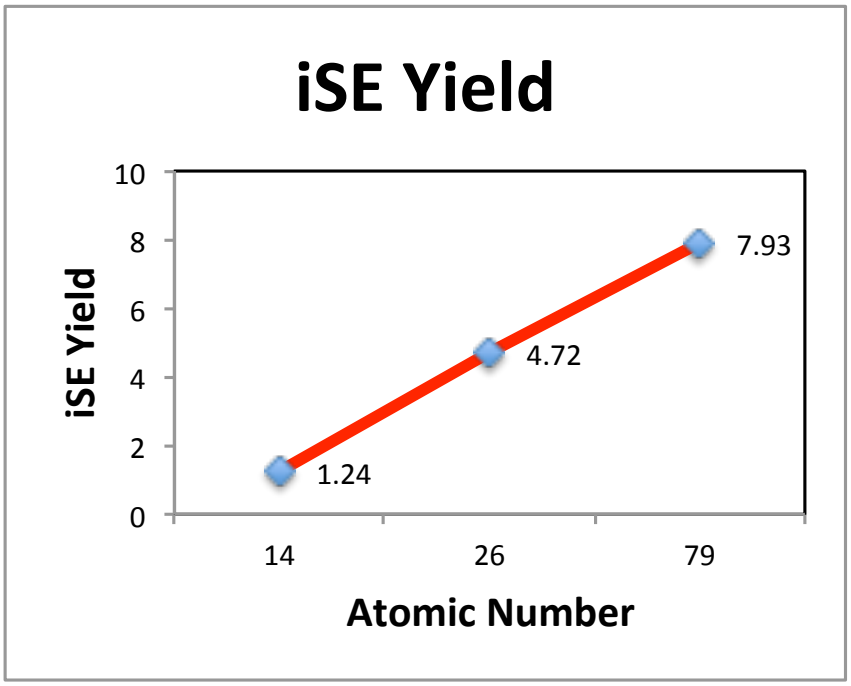


Figure 4.12. IONiSE aided-simulated iSE yield

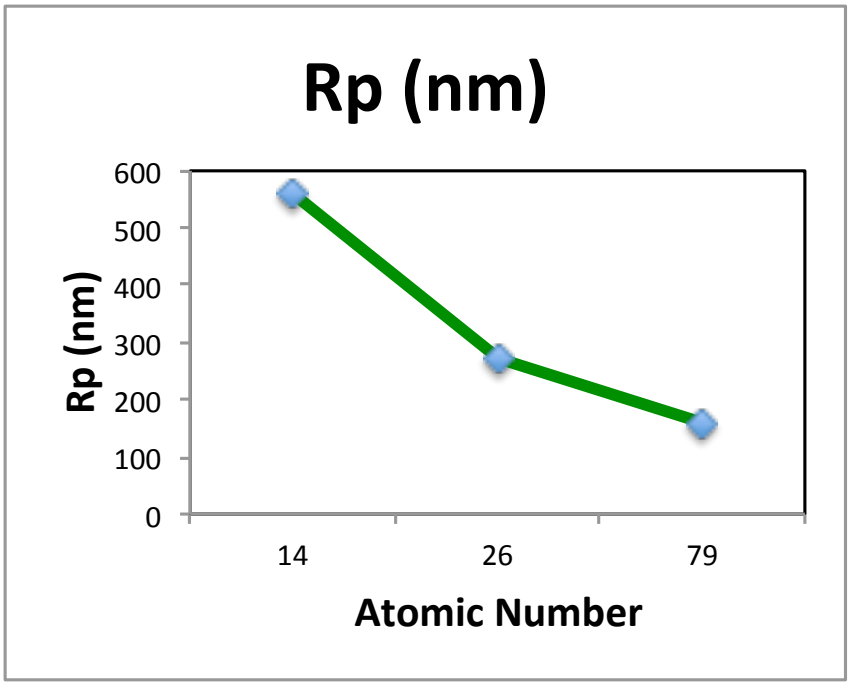


Figure 4.13. IONiSE aided-simulated projected range (nm)

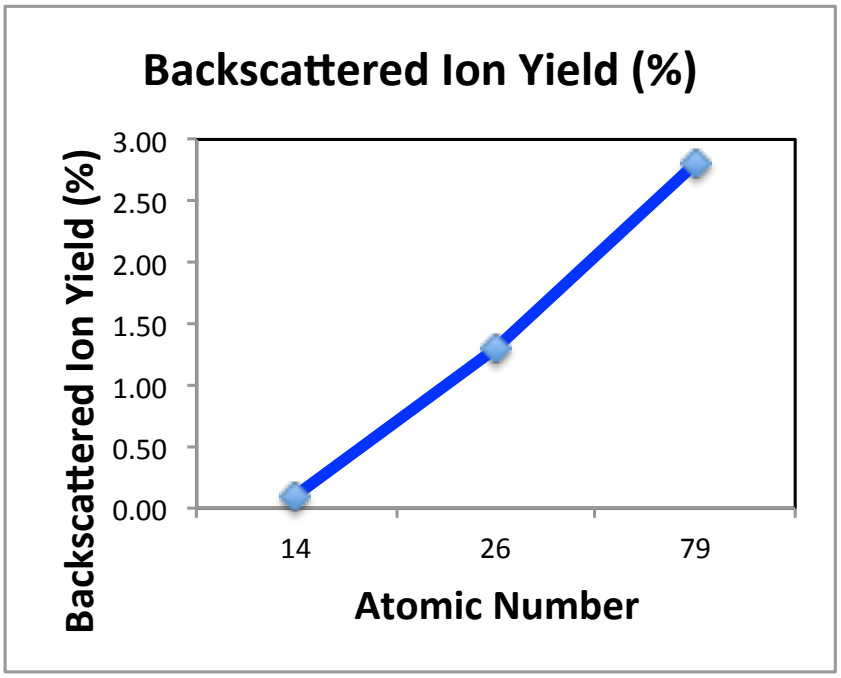


Figure 4.14. IONiSE aided-simulated backscattered ion yield (%)

For calculation of iSE yields for compound, the most popular contemporary materials are chosen as SiC, GaN, GaAs, $MoS_2$, InP, and GaSb among many of composite materials. Any of binary compounds can be chosen in the IONiSE software to compute secondary electron yields, projected range, and backscattered ion yield. The tabulated results are firstly pioneered outcomes given by the Monte Carlo Simulation technique incorporated with the universal ASTAR curve of helium stopping power. Validity of these results may not be true, however given that no accurate reliable experimental data for stopping power of each compound materials is available, at the same time, there is not any valid ground to disprove my approach is totally wrong. The approach is a big step forward and the best what we can obtain given current scientific fundamental. As continual update of high quality of experimental data of stopping power for certain compounds is made, immediate fitting to the individual reported experimental data, whenever the experimental data comes to be available, will replace the currently computed estimates

of iSE yield for the individual material and make the IONiSE software to be a more powerful semi empirical model for secondary electron production.

Table 4.2. IONiSE aided-simulated iSE yield, projected range, and backscattered yield values of incident helium ion beam for compounds

| Incident Ion | Helium (40 keV) | iSE Yield | $R_P$ (nm) | Backscattered Ion Yield (%) |
|---|---|---|---|---|
| Compound | SiC | 0.26 | 570 | 0.20 |
| | GaN | 0.18 | 1,070 | 1.20 |
| | GaAs | 0.36 | 330 | 5.40 |
| | $MoS_2$ | 0.46 | 600 | 3.20 |
| | InP | 0.77 | 650 | 5.10 |
| | GaSb | 0.91 | 300 | 9.90 |

# Chapter 5

## Conclusions and Recommendations

Recently commercialized helium ion microscope (HIM) has significant advantage over the scanning electron microscope (SEM) and its usefulness in a wide variety of applications will be more weighted, and not only nanotubes, nanowires, nanoparticles, polymers, multi-layered fabricated devices, and three dimensional biological materials but also further application in many of unknown realm will going to be introduced. However, not like the SEM, the performance of the HIM has not been fully quantified. For taking full advantage of the HIM, understanding capability and limit of the machine is essential. To quantify performance of the recently commercialized helium ion microscope, building a quantitative model of ion- solid interactions is necessary. Ion beam induced secondary electron yield (iSE δ) is one of the most important parameters to enable imaging of helium and different types of ion microscope and to mainly influences quality of imaging of microscopes.

To predict and interpret generation of secondary electrons by ions for matters in reliable precision, Monte Carlo simulation has been known for one of the best statistical method to simulate scattering events of energetic ion behavior in matter due to fast and accurate calculation for the complex ion beam interactions with matter. To enhance the Monte Carlo simulation, more accurate information of ion stopping power tables for wide range of materials is necessary. However, not enough theoretical data and almost total absent data of ion stopping power for pure elements and, even further, compounds has been reported. Given extremely limited current research environments where pursuing individual data tables for ion stopping power is plausible, having every sets of data tables through experiments are almost impossible. So, instead of relying on

hundreds of individual experimental data tables of helium stopping power, a recently calculated and published result by the group at NIST at Boulder is practically used.

Calculation of helium ion beam induced secondary electron behavior (iSE yield) within matters, not only elements but also compounds, should be able to be possible with newly constructed Monte Carlo simulation software (IONiSE), incorporated with the Universal ASTAR curve of stopping power for He ion. Using the IONiSE software, iSE yield could be computed as a function of energy of incident ion, and with a slight change in topography on the specimen surface for contribution to the current helium ion beam metrology. The predicted ion beam induced secondary electron behavior may not be accurate values, however given the almost absence of high quality experimental data of helium ion stopping power, understanding the iSE behavior of both elements and compounds is a pioneered work and there is no such a valid scientific ground to disprove the currently acclaimed approach.

Furthermore, our new approach should be able to handle not only helium ion beam but also other ion beams by simply changing the basic scattering profile. Hereby, it is believed that our new approach will be a milestone to enhance capabilities and performance of the currently commercialized helium ion microscope, and even further, other ion microscopes.

**List of References**

[1] M. Dapor, "Secondary electron emission yield calculation performed using two different Monte Carlo strategies," *Nuclear Instruments and Methods in Physics Research Section B: Beam Interactions with Materials and Atoms,* vol. 269, pp. 1668-1671, 2011.

[2] H. Paul. (2013). *Stopping Power for Light Ions*. Available: http://www.exphys.uni-linz.ac.at/stopping/

[3] F. Hubert, R. Bimbot, and H. Gauvin, "Range and stopping-power tables for 2.5–500 MeV/nucleon heavy ions in solids," *Atomic Data and Nuclear Data Tables,* vol. 46, pp. 1-213, 1990.

[4] Berger, "ICRU Report 49," 1993.

[5] J. F. Ziegler, *SRIM - The Stopping and Range of Ions in Matter*: Ion Implantation Technology, Incorporate, 2008.

[6] J. S. C. M.J. Berger, M.A. Zucker, J. Chang. *Stopping-Power and Range Tables for Electrons, Protons, and Helium Ions*. Available: http://www.nist.gov/pml/data/star/index.cfm

[7] L. Scipioni, L. A. Stern, J. Notte, S. Sijbrandij, and B. Griffin, "Helium ion microscope," *Advanced Materials & Processes,* vol. 166, pp. 27-30, Jun 2008.

[8] J. Notte, B. Ward, N. Economou, R. Hill, R. Percival, L. Farkas*, et al.*, "An introduction to the helium ion microscope," in *International Conference on Frontiers of Characterization and Metrology for Nanoelectronics*, Gaithersburg, MD, 2007, pp. 489-496.

[9] B. W. Ward, L. Farkas, J. A. Notte, and R. Percival, "SYSTEMS AND METHODS FOR A GAS FIELD IONIZATION SOURCE," USA Patent, 2008.

[10] D. C. Joy, "Scanning He plus Ion Beam Microscopy and Metrology," in *Frontiers of Characterization and Metrology for Nanoelectronics*, Grenoble, FRANCE, 2011.

[11] B. Arey, V. Shutthanandan, and W. Jiang, "Helium Ion Microscopy versus Scanning Electron Microscopy," W. R. Wiley Environmental Molecular Sciences Laboratory, Pacific Northwest National Laboratory.

[12] C. E. Kliewer, C. C. Walters, C. Huynh, L. Scipioni, D. Elswick, R. Jonk*, et al.*, "Geological Applications of Helium Ion Microscopy," ExxonMobil Research and Engineering Co.2012.

[13] D. Bell, L. A. Stern, L. Farkas, and J. A. Notte, "Helium ion microscope: advanced contrast mechanisms for imaging and analysis of nanomaterials," in *EMC 2008 14th European Microscopy Congress 1–5 September 2008, Aachen, Germany*, M. Luysberg, K. Tillmann, and T. Weirich, Eds., ed: Springer Berlin Heidelberg, 2008, pp. 527-528.

[14] D. E. N. Joseph Goldstein, David C. Joy, Charles E. Lyman, Patrick Echlin, Eric Lifshin, Linda Sawyer, J.R. Michael, *Scanning Electron Microscopy and X-ray Microanalysis*, 3rd ed.: Springer, 2003.

[15] . *Detection of signals*. Available: http://www4.nau.edu/microanalysis/Microprobe-SEM/Signals.html

[16] H. Seiler, "EINIGE AKTUELLE PROBLEME DER SEKUNDARELEKTRONENEMISSION," *Zeitschrift Fur Angewandte Physik,* vol. 22, pp. 249-&, 1967.

[17] . *Secondary electrons*. Available: http://www.emal.engin.umich.edu/courses/semlectures/se1.html

[18] B. D. Milbrath, A. J. Peurrung, M. Bliss, and W. J. Weber, "Radiation detector materials: An overview," *Journal of Materials Research,* vol. 23, pp. 2561-2581, Oct 2008.

[19] . *Chemistry@TutorVista*. Available: http://chemistry.tutorvista.com/nuclear-chemistry/rutherford-scattering.html

[20] D. C. Joy, *Monte Carlo Modeling for Electron Microscopy and Microanalysis*. New York: Oxford University Press, Inc., 1995.

[21] . *Specimen Interaction Volume during Microanalysis*. Available: http://www.globalsino.com/micro/1/1micro9992.html

[22] Y. W. Zhang and W. J. Weber, "Box 1: Stopping of Ions in Nanomaterials," *Ion Beams in Nanoscience and Technology,* pp. 87-93, 2009.

[23] W. J. Weber, "Energy Loss Theory and Stopping Power (Lecture 6)," ed, 2011.

[24] D. C. Joy, "AN INTRODUCTION TO MONTE-CARLO SIMULATIONS," *Scanning Microscopy,* vol. 5, pp. 329-337, Jun 1991.

[25] R. Ramachandra, B. Griffin, and D. Joy, "A model of secondary electron imaging in the helium ion scanning microscope," *Ultramicroscopy,* vol. 109, May 2009.

[26] J. P. Biersack and L. G. Haggmark, "A MONTE-CARLO COMPUTER-PROGRAM FOR THE TRANSPORT OF ENERGETIC IONS IN AMORPHOUS TARGETS," *Nuclear Instruments & Methods,* vol. 174, pp. 257-269, 1980.

[27] O. B. Firsov, "CALCULATION OF THE INTERACTION POTENTIAL OF ATOMS," *Soviet Physics Jetp-Ussr,* vol. 6, pp. 534-537, 1958.

[28] J. Lindhard, V. Nielsen, and M. Scharff, "APPROXIMATION METHOD IN CLASSICAL SCATTERING BY SCREENED COULOMB FIELDS," *Matematisk-Fysiske Meddelelser Udgivet Af Det Kongelige Danske Videnskabernes Selskab,* vol. 36, pp. 3-&, 1968 1968.

[29] J. F. Ziegler, J. P. Biersack, and U. Littmark, *The Stopping and Range of Ions in Solids* vol. null, 1985.

[30] K. B. Winterbon, *Spatial distribution of energy deposited by atomic particles in elastic collisions*. Munksgaard: København, 1970.

[31] G. P. Mueller, "TOTAL CROSS-SECTION CORRESPONDING TO DIFFERENTIAL CROSS-SECTION OF LINDHARD, NIELSEN AND SCHARFF," *Radiation Effects and Defects in Solids,* vol. 21, pp. 253-254, 1974.

[32] E. J. Sternglass, "THEORY OF SECONDARY ELECTRON EMISSION BY HIGH-SPEED IONS," *Physical Review,* vol. 108, pp. 1-12, 1957.

[33] N. Benazeth, "REVIEW ON KINETIC ION-ELECTRON EMISSION FROM SOLID METALLIC TARGETS," *Nuclear Instruments & Methods in Physics Research,* vol. 194, pp. 405-413, 1982.

[34] A. Dubus, J. Devooght, and J. C. Dehaes, "A THEORETICAL EVALUATION OF ION INDUCED SECONDARY-ELECTRON EMISSION," *Nuclear Instruments & Methods in Physics Research Section B-Beam Interactions with Materials and Atoms,* vol. 13, pp. 623-626, Mar 1986.

[35] T. Ishitani, A. Shimase, and S. Hosaka, "MONTE-CARLO SIMULATION OF ENERGETIC ION BEHAVIOR IN AMORPHOUS TARGETS," *Japanese Journal of Applied Physics Part 1-Regular Papers Short Notes & Review Papers,* vol. 22, pp. 329-334, 1983.

[36] Y. Sakai, T. Yamada, T. Suzuki, T. Sato, H. Itoh, and T. Ichinokawa, "Contrast mechanisms in scanning ion microscope imaging for metals," *Applied Physics Letters,* vol. 73, Aug 3 1998.

[37] K. Inai, K. Ohya, and T. Ishitani, "Simulation study on image contrast and spatial resolution in helium ion microscope," *Journal of Electron Microscopy,* vol. 56, pp. 163-169, Oct 2007.

[38] H. A. Bethe, "On the theory of Secondary Emission," *Physical Review,* vol. 59, pp. 940-941, 1941.

[39] M. R. Scheinfein, J. Drucker, and J. K. Weiss, "Secondary-electron production pathways determined by coincidence electron spectroscopy," *Physical Review B,* vol. 47, pp. 4068-4071, 1993.

[40] J. Ferron, E. V. Alonso, R. A. Baragiola, and A. Olivaflorio, "DEPENDENCE OF ION-ELECTRON EMISSION FROM CLEAN METALS ON THE INCIDENCE ANGLE OF THE PROJECTILE," *Physical Review B,* vol. 24, 1981 1981.

[41] H. Salow, "On the angle dependency of secular electron emissions of isolators," *Physikalische Zeitschrift,* vol. 41, pp. 434-442, 1940.

[42] W. H. Press, *Numerical Recipes 3rd Edition: The Art of Scientific Computing*. New York: Cambridge University Press, 2007.

[43] (2004). *How Visual Basic Generates Pseudo-Random Numbers for the RND Function*. Available: http://support.microsoft.com/kb/231847

## Vita

Uk Huh was born in Shimonoseki, Japan, on June 19, 1975. He obtained his B.S. degree in Metallurgical Engineering in the year 2000 from Yonsei University, Seoul, South Korea. From 2000 to 2004, he worked as a PECVD engineer, a quality control engineer, and an overseas sales specialist for AMLCD (Active Matrix Liquid Crystal Display) Division of Samsung Electronics Co., Ltd. He resumed his education in Industrial Engineering in the year of 2005 from North Carolina State University, U.S.A. and earned his M.S. degree in Material Science and Engineering in the year of 2008 from the same institute as there was a switch of his major to Material Science and Engineering in 2006. Uk transferred to the University of Tennessee, Knoxville in the year of 2009 to pursue his Ph.D. degree and will earn the degree under direction of Professor David Joy's direction in August 2014.